Author accepted version. Final publication as:
Khorsandi, B., Gaskin, S.J. & Mydlarski, L.M. (2013) Effect of background turbulence on an axisymmetric turbulent jet, Journal of Fluid Mechanics, 736:250–286. doi: http://dx.doi.org/10.1017/jfm.2013.465

Effect of background turbulence on an axisymmetric turbulent jet

B. KHORSANDI[1], S. GASKIN[1] AND L. MYDLARSKI[2]

[1]Department of Civil Engineering and Applied Mechanics, McGill University, 817 Sherbrooke Street West, Montréal, QC, H3A 0C3, Canada

[2]Department of Mechanical Engineering, McGill University, 817 Sherbrooke Street West, Montréal, QC, H3A 0C3, Canada

(Received ?? and in revised form ??)

The effect of different levels of background turbulence on the dynamics and mixing of an axisymmetric turbulent jet at different Reynolds numbers was investigated. Approximately homogeneous and isotropic background turbulence was generated by a random jet array and had a negligible mean flow ($\langle U_\alpha \rangle / u_{\alpha rms} \ll 1$). Velocity measurements of a jet issuing into two different levels of background turbulence were conducted for three different jet Reynolds numbers. The results showed that the mean axial velocities decay faster with increasing level of background turbulence (compared to a jet in quiescent surroundings), while the mean radial velocities increase, especially close to the edges of the jet. Furthermore, the axial RMS velocities of the jet increased in the presence of background turbulence, as did the jet's width. However, the mass flow rate of the jet decreased, from which it can be inferred that the entrainment into the jet is *reduced* in a turbulent background. The effect of background turbulence on the entrainment mechanisms is discussed.

1. Introduction

Industrial activities often result in large quantities of pollutants being discharged into the atmosphere and hydrosphere (rivers, lakes, oceans) in the form of turbulent jets or plumes. These damage the ecosystem and endanger human health. Dilution of the pollutants, by entrainment and mixing with the ambient fluid, reduces their acute toxic effects. A higher initial dilution can minimize the immediate toxic effect near the point of release and leads to higher dilutions (lower concentrations) downstream. These impacts motivate this study, given that the vast majority of the research on jets has been carried out in quiescent or laminar background flows, so their results may not be valid for discharges into turbulent environments (as is the case for most environmental and industrial flows).

The dynamics of a jet and its entrainment both depend on the jet parameters, as well as those of the environment/receiving fluid. The latter ones include: i) the presence and/or level of background turbulence, ii) mean flow advection, iii) density stratification, and iv) the presence of boundaries. Given the complexity in accounting for the above-mentioned environmental parameters, it is initially beneficial to study their individual effects on the dilution of a jet. We therefore propose to study a jet emitted into a turbulent background to predict and characterize the effect of environmental turbulence. Before doing so, we present a brief review of turbulent jets emitted into a quiescent background, followed by a discussion of jets emitted into a turbulent background. In both cases, the question of the mechanism and rate of entrainment into jets will be considered.

Axisymmetric turbulent jets in a quiescent background are two-dimensional free shear flows, dependent on the axial (x) and radial (r) positions. The profiles of the mean (axial and radial) velocity and Reynolds (normal and shear) stresses decay (in x) and spread (in r), becoming self-similar after an initial development region, with the mean veloc-

ity reaching a self-similar state before the Reynolds stresses (Wygnanski and Fiedler, 1969). A theoretical analysis, using either the equations of motion (continuity and axial momentum) with the boundary layer approximations, or dimensional analysis yields the scaling behaviours of the mean axial velocity and transverse length scale (generally quantified in terms of the jet half-width – Pope, 2000). The mean centreline axial velocity scales inversely with downstream distance ($\langle U_{CL} \rangle \propto x^{-1}$) while the jet half-width scales with downstream distance ($r_{1/2} \propto x^1$), with each *nominally* independent of the initial Reynolds number, and resulting in a constant local Reynolds number. (See George (1989) or Hussein, Capp and George (1994) for more on this.) Consequently the mass flow rate ($\propto \langle U_{CL} \rangle r_{1/2}^2$) increases linearly with downstream distance. Furthermore, the root-mean-square of the axial centreline velocity fluctuation, normalized by the mean axial centreline velocity, asymptotes to a constant (0.24-0.28) after a certain downstream distance. Assuming self-similarity, Morton, Taylor and Turner (1956) introduced the entrainment assumption, which states that the entrainment rate is proportional to a local characteristic velocity in the jet, such that the details of the turbulent mixing need not be known.

Subsequent to the work of Morton, Taylor and Turner (1956), the entrainment mechanisms of jets emitted into quiescent backgrounds were studied more extensively. In the zone of flow establishment of an axisymmetric turbulent jet, there is large-scale entrainment by organized vortical structures, shed from the discharging flow, and similar to those seen in shear layers. However, these vortex rings breakdown within a few jet diameters downstream of the exit. This initial development region is followed by the near-field of the jet (where the jet becomes self-similar). In this region, two main entrainment mechanisms have been proposed: engulfment and nibbling.

Engulfment is a large-scale inviscid process in which large volumes of ambient fluid are

drawn into the shear flow by large eddies. Subsequent mixing is carried out by viscous diffusion of vorticity (e.g., Townsend, 1956; Brown and Roshko, 1974). Flow visualization and measurements of the scalar concentration field by Dahm and Dimotakis (1987, 1990) confirm the existence of entrainment by engulfment and show that the entrainment and mixing processes in the near-field of a turbulent jet can be characterized by scales approximately equal to the local large scales of the flow. The instantaneous concentration profiles from their work also show that (unmixed) ambient fluid is transported deep into the jet. This is argued to be further evidence of large-scale entrainment.

Nibbling, on the other hand, is a small-scale, viscous process that occurs by small-scale eddies at the very thin interface (on the order of the Kolmogorov microscale thick; Corrsin and Kistler, 1955) between the turbulent and non-turbulent flows. This interface or "laminar super-layer" plays a significant role in transmitting vorticity to the irrotational fluid by tangential viscous (and not macroscopic shear) forces, unlike momentum transfer, which is dominated by velocity fluctuations (Corrsin and Kistler, 1955). Although there exists a debate as to the relative importance of the two processes, direct numerical simulations by Mathew and Basu (2002), have shown nibbling to be the dominant entrainment process. In their simulations, they defined a vorticity threshold level. If the threshold was crossed, the fluid was deemed part of the turbulent jet. If engulfment were the dominant mechanism, i) there should exist areas within the jet with vorticity levels below that of the threshold, and ii) the positions where the threshold was surpassed should be distributed within the jet. They, however, concluded that nibbling was the main entrainment mechanism, as the threshold was mostly crossed at the interface. Mathew and Basu's (2002) conclusions were also recently corroborated experimentally by Westerweel *et al.* (2009), who found that nibbling at the interface is effected by small

scale-eddies and that the engulfed mass consisted of less than 10% of the total entrained mass.

Regardless of the entrainment mechanism, as long as scale-similarity exists (as is the case in a self-similar jet emitted into a quiescent background), the overall rate of entrainment can be predicted by characteristic (large or small) scales of the flow. However when the jet turbulence is not in equilibrium (e.g., when turbulence in the ambient flow disrupts the jet structure and, consequently, the relation between the scales), the entrainment mechanism and the conditions under which the assumption of self-similarity remain valid need to be re-investigated (Mathew and Basu, 2002).

Hunt (1994) theoretically reasoned that an increased mass or momentum flow rate of a jet will increase entrainment, whereas any tendency of the jet to break up into distinct eddies will decrease it. He hypothesized that the disruptive effect of background turbulence would decrease the entrainment into a jet. This hypothesis was confirmed experimentally by Gaskin *et al.* (2004) for a plane jet in a shallow co-flow, in which the co-flow was intensified by placing ribs across the channel bed. Measurements of both velocity and concentration confirmed a decreased entrainment in the presence of ambient turbulence.

Conversely, as part of a study of jets in shallow co-flows with different bed roughnesses, Wright (1994) hypothesized that the entrainment by the jet and that due to the ambient turbulence would be additive and lead to an increase in the total entrainment rate. The experimental results, in which the entrainment increased with the level of free-stream turbulence, showed significant scatter, especially in the case of a low ratio of the jet and ambient velocities.

Other studies have investigated momentum jets (Guo *et al.*, 1999; Law *et al.*, 2001; Guo *et al.*,2005), buoyant jets (Cuthbertson *et al.*, 2006) or plumes (Ching *et al.*, 1999)

in background turbulence. Measurements of both velocity and concentration found that the jet/plume was destroyed and the spreading rate increased once a certain level of background turbulence intensity was reached. The critical turbulence level varied in the different works, and was found to occur when the RMS of the background turbulence was on the order of the plume velocity (Ching *et al.*, 1999), approximately 0.125 of the jet velocity (Guo *et al.*, 1999), on the order of the RMS of the jet (Guo *et al.*,2005) or plume (Cuthbertson *et al.*, 2006), or when the jet was close to the grid (Law *et al.*, 2001). However, the jet/plume axis in these studies was oriented perpendicular to the oscillating grid such that the level of background turbulence increased in the downstream direction (of the jet/plume). Close to the jet exit, the background turbulence is weak, so it has little effect on the jet structure, as observed by Law *et al.*, (2001). However, close to the grid, the intensity of the background turbulence is higher than that of the decaying jet and was observed to have a significant influence. In such an experimental arrangement, the jet/plume is also blocked by the oscillating grid, resulting in accumulation of mass near the grid (as observed by Law *et al.*, (2001) and Ching *et al.* (1995)), which explains the sudden increase in spreading and entrainment rates close to the grid. The characteristics of these experiments render the conclusions thus obtained ambiguous.

In addition, in the studies of plane jets in shallow co-flows (e.g., Wright, 1994; Gaskin *et al.*, 2004), the presence of mean-flow advection and the shallowness of the channel can affect the structure of the turbulent jet. Consequently, a thorough and systematic study of jets issuing into a homogenous isotropic turbulent background (with zero-mean flow) is required to further characterize jets in turbulent backgrounds, and to also confirm or refute the above hypotheses.

An experimental investigation into the effect of the level of background turbulence on the velocity field of a momentum-driven, axisymmetric, turbulent jet is presented herein.

An approximately homogeneous, isotropic turbulent background with zero mean flow was generated by a random jet array (RJA) in a water tank (Variano *et al.*, 2004, Variano and Cowen, 2008). In this study, the jet was issued parallel to the RJA plane, resulting in a quasi-homogeneous turbulent intensity in the background flow along the axis of the jet (unlike the previously-mentioned experiments).

The remainder of this paper is structured as follows. The details of the experimental setup are presented in §2. For the purposes of validation of the experimental methods employed herein, the statistics of a jet issuing into a quiescent background are compared to those of the previous studies in §3. In §4.1, measurements of the background turbulence are presented. §4.2 treats results pertaining to the effect of different levels of background turbulence on the jet. Lastly, a discussion of the results is presented in §5.

2. Experimental apparatus

The description of the background conditions, jet apparatus, and the acoustic Doppler velocimetry (ADV) and flying hot-film anemometry systems is given below. For additional details, the reader is referred to Khorsandi (2011).

2.1. *Background conditions*

The experiments were conducted in a sub-section of an open glass (walls and bottom) and steel-framed tank (1.5 m by 6 m by 1 m) filled with water. The tests were carried out in either i) a quiescent background, or ii) an approximately homogeneous, isotropic turbulent background with zero mean flow. The latter was generated by a random jet array (RJA) based on that of Variano *et al.* (2004) and Variano and Cowen (2008), built to a larger scale in the 1.5 m by 2.4 m by 0.9 m sub-section of the tank (Figure 1). The turbulence generated by an RJA creates a lower mean flow than that generated by an oscillating grid (Variano and Cowen, 2008). The RJA consists of an array of 6×10 bilge

pumps (Rule 25D, 500 GPH) mounted on a 1 m by 1.5 m vertical sheet of high density polyethylene. The pumps take in water radially at their base and discharge it axially via a 0.15 m long, 31.75 mm diameter extension tube perpendicular to and 0.24 m from the plane of the RJA. The pump spacing is uniform with a centre-to-centre distance (M) of 150 mm, and employs reflectional symmetry at the walls to lessen the possibility of secondary circulations (Fernando and De Silva, 1993; Variano *et al.*, 2004; Variano and Cowen, 2008). Downstream of the RJA, the jets merge, creating an approximately homogeneous isotropic turbulent flow with almost zero mean flow. The RJA is operated using an algorithm to independently and randomly turn the pumps on and off, programmed in LabVIEW. The algorithm providing the optimal flow conditions (in terms of low mean velocity, and highest degrees of homogeneity and isotropy) controlled the pump operation using two normal distributions, defined by their mean and standard deviation, to set the pump on- and off-times (Variano and Cowen, 2008). The normal distribution parameters were $(\mu_{on}\ ,\ \sigma_{on}) = (12\ ,\ 4)$ s, and $(\mu_{off}\ ,\ \sigma_{off}) = (108\ ,\ 36)$ s, which resulted in 10% of the pumps being on at any given time (on the average). This produced a superior flow to an alternate algorithm (Khorsandi, 2011), in which the state of a pump changed if a random number (between 0 and 1) generated every 0.4 seconds (for each pump) was greater than a certain threshold (0.98) (Mydlarski and Warhaft, 1996). As the first algorithm generated a superior flow quality, it was employed in all further experiments.

2.2. *Jet apparatus*

An axisymmetric turbulent jet of circular cross section issued into the water tank (parallel to the RJA), supplied from a constant-head source and precisely positioned by a traversing mechanism. The constant-head (of 2 m), maintained by overflows, assured a constant jet flow rate. The supply for the constant head reservoir was the main tank for the flying hot-film measurements and a separate clean water supply for the ADV mea-

surements (due to particles added to the main tank water to increase the signal-to-noise ratio of the measurements). See Figure 1 of Lavertu, Mydlarski and Gaskin (2008) for a schematic of the tank, constant-head reservoir and jet components.

The jet flow was fed from the constant-head reservoir via flexible tubing to an 8 mm diameter L-shaped jet (in copper tubing). A flow meter (Omega FL50002A) maintained a flow rate between 2-4 litres/min, corresponding to Reynolds numbers of 5,300-10,600 for an 8 mm diameter jet, with a ball valve to set the flow rate and a solenoid valve to turn the flow on and off, placed before and after it, respectively. The L-shaped jet was mounted on a traversing mechanism and extended vertically for 1.6 m and, after a 90° bend, horizontally for 0.12 m (15 jet diameters). At the jet exit, the flow was fully-developed. Statistics in the self-similar region (where the majority of our results are recorded) are not affected by the initial conditions (Ferdman *et al.*, 2000; Xu and Antonia, 2002). The jet was positioned parallel to the plane of the RJA so that the turbulence generated by RJA was homogeneous along the axis of the jet.

For each jet experiment, the probe was precisely aligned with the jet axis, as determined from vertical and horizontal profiles measured by the ADV or hot-film probe. Subsequent radial measurements were carried out in small increments from the jet centreline towards its edges. The radial measurements were made in the vertical (z) direction so that the turbulence generated by the RJA was homogeneous along the radius.

Traversing mechanisms were required to move the jet and/or probe so that measurements could be carried out at several points in the radial and axial directions. During the ADV measurements, the jet was fixed and the measurement apparatus was moved precisely horizontally and vertically (along the radius: y- and z-directions) and also along the axis of the jet (x-direction), using a Velmex traversing mechanism. For the flying hot-film measurements, the jet was moved horizontally and vertically (y- and z-direction) with

the Velmex traversing mechanism, while the probe was translated at high velocities along the axis of the jet in the x-direction, with its instantaneous position also provided, using a high-precision Aerotech traversing mechanism (described below).

2.3. *ADV apparatus*

The acoustic Doppler velocimetry measurements were made with a Nortek Vectrino 10-MHz acoustic Doppler velocimeter. The accuracy of the velocity signal measured by the ADV is 0.5% of the sampling range, which was selected to be ± 10, ± 30 or ± 100 cm/s (depending on the flow being measured), to span the entire range of measured velocities for the experiments. The sampling rate was set to 25 Hz (the maximum). The sampling volume of the ADV, located 5 cm below the probe (minimizing flow interference by the probe), was set to its maximum volume of 0.26 cm^3 and the ADV power level was set to High, providing the maximum signal-to-noise ratio (SNR). Because the ADV operates by measuring acoustic signals reflected off particles in the flow, neutrally buoyant glass particles (Potters Industries Sphericel hollow glass spheres of 9-13 μm diameters) were added to the water to increase the SNR of the ADV. The ADV parameters were set and the data were acquired using the manufacturer's software.

For each test, the velocity range was set and the quality of the data ensured by checking that the SNR and correlation parameters were above the minima specified by the manufacturer of 15 dB and 70%, respectively. For the measurements of the background turbulence generated by the RJA, the SNR was greater than 20 dB and the correlation was 99% at all times. For the measurements of the jet, the SNR and the correlation dropped significantly close to the jet exit ($x/D < 30$), because the jet water did not contain particles. At distances greater than $x/D > 30$, as the jet mixed and entrained ambient fluid (and therefore particles), the SNR and the correlation increased to higher than 20 dB and 70%, respectively.

2.4. *Flying hot-film anemometry apparatus*

For stationary hot-film anemometry measurements, the presence of (and knowledge of the direction of) the mean velocity is required, as heat transfer (which is a scalar) is measured, which does not account for the flow direction. Consequently, when the mean flow is small compared to the magnitude of the turbulent fluctuations, or when reversing flows are known to be present, thermal anemometry measurements are inaccurate. In the present experiments, this was true i) at the edges of the jet during the quiescent background experiments, ii) during measurement of the background turbulence generated by the random jet array, and iii) within a jet emitted into background turbulence. To overcome this limitation, the hot-film probe was translated at a constant speed using a traversing mechanism designed and built for the purpose of inducing an artificial mean flow. The velocity of the traversing mechanism was chosen so that $u_{rms}/\langle U \rangle < 0.2$ — in analogy with the upper limit for the applicability of Taylor's frozen flow hypothesis. This artificial mean velocity was later subtracted from the measured velocity data. During calibrations of the hot-film anemometer, the probe was moved at velocities ranging from 0.01 m/s to 1.1 m/s. For all other experiments, the probe was moved at a constant velocity of 0.1-0.3 m/s.

The flying hot-film anemometry apparatus consisted of an Aerotech high-precision linear traversing mechanism, a TSI 1210-20W hot-film sensor connected to a DISA 55M10 constant-temperature anemometer, a Krohn-Hite (Model 3382) filter for the low-pass filtering of the data, and a data acquisition unit (for use with the traversing mechanism) for recording the position and velocity of the sensor.

The output voltages of the hot-film anemometer were available at intervals of 1 μm along the jet axis from $x/D = 10$ to $x/D = 115$. (x was the distance downstream of the jet, and D was the exit diameter of the jet nozzle). Each pass of the traversing mecha-

nism provided one data point for a given x/D downstream of the jet. Tests showed that statistical convergence of the data measured in i) the jet in quiescent flow, ii) the background turbulence generated by the RJA, and iii) the jet in the presence of background turbulence was obtained for 1000, 300, and 1200 data points (passes), respectively.

The Aerotech traversing mechanism consisted of a carriage running along a (1248 mm long) monorail, and driven by a linear motor guided by a magnet track parallel to the monorail. An encoder on the carriage gave the carriage position (with a spatial resolution of 1 μm) which was also a feedback to the control system. The hot-film probe was fixed to the carriage. To decrease the drag and reduce probe oscillations induced by vortex shedding from the immersed rod, the bottom 45-cm of the probe was a stainless steel cylinder of an airfoil cross-section (length = 50 mm, width = 22 mm). The hot-film probe was mounted on a circular rod fixed perpendicular to the front of the lower end of the airfoil, with the hot-film sensor's tip 18 cm in front of the airfoil shaped rod.

The hot-film anemometry measurements required clean water with a controlled water temperature. The water supplied to the tank was filtered with a coarse sand filter in series with a fine diatomite filter (2 μm). Once filled, it was filtered continuously with the fine filter in a recirculation loop. Algaecide was also added to the water. This minimized the (hot-film) probe fouling. The hot-film probe was also carefully cleaned with a fine brush and calibrated before and after each test. Before each test the water was heated to room temperature (while being recirculated and filtered). The temperature of the water was monitored and recorded before and after each test to an accuracy of ± 0.1 °C (with the maximum variation being ± 0.3 °C per 12 hour period).

Data was collected at a deterministic rate with no delays using a field-programmable gate array (FPGA) card that was independent of the data acquisition computer's operating system. The voltage data from the flying hot-film anemometer and position data

were acquired simultaneously. The analogue anemometer output signal was converted to a digital signal while the position data was digital (Khorsandi 2011).

LabVIEW FPGA programs ("virtual instruments") were developed for i) calibration, and ii) controlling the data acquisition and the motion of the traversing mechanism. The voltage of the anemometer and the digital signal of the encoder were each acquired at the maximum sampling rate of 100 kS/s and 2 MS/s, respectively. They were subsequently acquired instantaneously in a "Host" program with a sampling frequency of 1 kHz. Low-pass filtering, at 500 Hz in accordance with the Nyquist criterion, of the output voltage of the hot-film anemometer was used to remove all noise from frequencies higher than the maximum frequency in the (turbulent) flow.

A relationship between the output voltage of the hot-film anemometer and the fluid velocity was determined using King's Law ($E^2 = A + BU^n$, where E is the anemometer output voltage, U is the fluid velocity, and A, B and n are calibration constants). Calibration data were obtained by moving the probe at different velocities in stationary water.

Drift in the hot-film anemometer's calibration was minimized by the continuous filtering the water, use of an algae inhibitor, and the heating of the water to room temperature prior to the calibration. To monitor drift, two calibrations, one immediately before and one immediately after each test, were conducted. If any significant shift in the calibration (due to the water temperature change and/or probe contamination) was observed, the calibration and experiment were repeated. Otherwise the average voltage of the two calibrations was used to determine the calibration constants for the entire experimental run.

3. Validation of flow measurements

Experiments validating the acoustic Doppler velocimetry and the flying hot-film anemometry measurements are presented in this section. Specifically, the axial and radial variations of the mean and RMS velocities as well as, the spreading and entrainment rates of an axisymmetric turbulent jet issuing into a *quiescent* background, measured by both ADV and flying hot-film anemometry (FHFA), are compared with stationary hot-film anemometry (SHFA) measurements, as well as those of previous researchers. The latter include the i) stationary hot-wire anemometry (SHWA) measurements of Wygnanski and Fiedler (1969), ii) flying hot-wire anemometry (FHWA) measurements of Panchapakesan and Lumley (1993) and iii) SHWA, FHWA and laser Doppler anemometry (LDA) measurements of Hussein, Capp and George (1994).

The downstream evolution of the inverse of the normalized mean axial centreline velocity of the jet ($U_J/\langle U_{CL}\rangle$, where U_J is the nozzle exit velocity) is plotted in Figure 2 as a function of x/D (where D is the exit diameter of the nozzle). The present ADV and flying hot-film anemometry data (as well as stationary hot-film anemometry data) are compared with the results of Wygnanski and Fiedler (1969), Panchapakesan and Lumley (1993) and Hussein, Capp and George (1994). As can be seen, the mean centreline axial velocity measurements using ADV, and stationary and flying hot-film anemometry agree well with those of the other studies. (However, note that the flying hot-film anemometry data diverge from the previous research far downstream where the jet velocities become especially small. This may be related to inaccuracies in thermal anemometry techniques at low speeds, due to erroneously large velocities being recorded when natural convection effects are no longer negligible when compared to those of forced convection.)

The mean axial velocity is found to vary inversely with the downstream distance in the self-similar region, such that: $\langle U_{CL}(x)\rangle/U_J = B/[(x - x_0)/D]$, where x_0 is the virtual

origin of the jet and B is the decay constant. The present estimates of B are compared with those from previous experiments in Table 1. Their values (which depend on the particular choice of virtual origin, x_0/D), are consistent with previous research, thus confirming the accuracy of the present ADV and FHFA apparatuses for mean flow measurement (at least up to $x/D \approx 90$). Note that a virtual origin of zero is used when plotting the present data in all plots herein.

The radial profile of the axial mean velocity measured at $x/D = 35$ is presented in Figure 3. Given that it was not possible to extract the raw data of Panchapakesan and Lumley (1993) — a curve fit to their data is shown in this graph. The mean velocity profiles measured using the FHFA and ADV are in very good agreement with those of Wygnanski and Fiedler (1969), Panchapakesan and Lumley (1993) and Hussein, Capp and George (1994), with the present FHFA data being somewhat closer to that of the previous works than the ADV data. The lower values of the ADV data may be due to the larger sampling volume of the ADV compared to that of the FHFA.

The radial profiles of the mean radial velocity measured by the ADV at $x/D = 35$ and 75 are shown in Figure 4. Similar to the radial profile of mean axial velocity, $\langle V(r)\rangle/\langle U_{CL}\rangle$ should have a universal profile in the self-similar region when plotted as a function of r/x. However, given that the magnitude of the radial velocities is small compared to the axial velocities – $\langle V(r)\rangle$ is less than $1/40^{th}$ of $\langle U_{CL}\rangle$ (Pope, 2000) – it has therefore been less commonly measured. Furthermore, Wygnanski and Fiedler (1969), Panchapakesan and Lumley (1993) and Hussein *et al.* (1994) do not present raw data for the mean radial velocity. In these studies, the $\langle V(r)\rangle$ data is calculated from the mean axial velocity profile using the continuity equation. Therefore in addition to our raw ADV data, we also present in Figure 4 the profile of the mean radial velocity inferred from the measured mean axial velocities in Figure 3, from both the ADV and the FHFA data. As observed in Figure

4, the ADV predicts $\langle V(r)\rangle$ consistently, when compared to previous estimates of $\langle V(r)\rangle$ obtained from the continuity equation. As would be expected, the agreement is improved when comparing radial profiles obtained from the continuity equation. Furthermore, the agreement is better at $x/D = 75$, because the jet has reached a higher degree of self-similarity at this larger downstream distance.

The half-width ($r_{1/2}(x)$) of the jet is defined as the radial position at which the velocity falls to half of its value at the centreline. In a quiescent background, $r_{1/2}$ grows linearly with the downstream distance in the self-similar region: $r_{1/2} = S(x - x_o)$, where S is defined as the jet spreading rate (Pope, 2000). The spreading rates measured herein are compared to the previous experiments listed in Table 1, and agree well. Note that the spreading rate is independent of the Reynolds number (Pope, 2000).

Mass flow rates ($m(x)$) were calculated by integrating the area under the radial profiles of mean axial velocity. The jet entrainment rates (i.e., dm/dx) were subsequently calculated and found to be 0.34 and 0.42 for the ADV and FHFA measurements, respectively. Ricou & Spalding (1961) and Panchapakesan and Lumley (1993) reported an entrainment rate of 0.32 ($m/m_0 = 0.32 \times x/D + x_0$, with $x_0 = 0$) for a round turbulent jet at $Re > 2.5 \times 10^4$ and $Re = 1.1 \times 10^4$, respectively. If we limit ourselves to the range $15 \leqslant x/D \leqslant 60$, the entrainment rate measured by the FHFA becomes 0.36. (The entrainment rate increases after $x/D = 60$, due to the low sensitivity of the hot-film at low velocities.) If the virtual origin (x_0) of the curve fits to the data is forced to zero (like Ricou & Spalding (1961)), entrainment rates of 0.30 and 0.38 (0.33 for $15 \leqslant x/D \leqslant 60$) are obtained for the ADV and FHFA, respectively.

Figure 5 plots the axial RMS velocity normalized by the mean velocity ($u_{rms}/\langle U_{CL}\rangle$) at the jet centreline. Similar to the mean velocity, the RMS velocity decays as x^{-1}. Therefore, RMS velocities normalized by mean velocities at the centreline asymptote

to a constant value in the self-similar region. Although some variations in this quantity have been observed in the literature, no systematic dependence on the Reynolds number has been found (Pope 2000). Wygnanski and Fiedler (1969), and Hussein, Capp and George (1994) measured $u_{rms}/\langle U_{CL}\rangle$ to be approximately 0.28 in the self-similar region, whereas Panchapakesan and Lumley (1993) measured a value of 0.24. In the present study, $u_{rms}/\langle U_{CL}\rangle$ at the centreline of the jet in the self-similar region is found about 0.27 when measured using both stationary and flying hot-film anemometry, while $u_{rms}/\langle U_{CL}\rangle$ measured by the ADV is about 0.35. The ADV significantly overestimates $u_{rms}/\langle U_{CL}\rangle$ while the flying hot-film anemometer measures this quantity accurately when compared to other studies. As the mean velocity along the centreline is predicted relatively accurately by the ADV, the overestimation must be due to erroneously large estimates of the RMS velocities, which are inherent to ADV. (See Nikora and Goring, 1998; Voulgaris and Trowbridge, 1998; Hurther and Lemmin, 2008; Khorsandi *et al.*, 2012 for more on the observed abnormally large noise levels in ADV measurements of u_{rms} and v_{rms}.)

Lateral RMS velocities normalized by the mean velocity ($v_{rms}/\langle U_{CL}\rangle$ and $w_{rms}/\langle U_{CL}\rangle$) measured by ADV at the jet centreline are plotted in Figure 6. By symmetry, v_{rms} and w_{rms} should be the same at the centreline of an axisymmetric jet, however the ADV measurements result in $v_{rms}/\langle U_{CL}\rangle \approx 0.30$ and $w_{rms}/\langle U_{CL}\rangle \approx 0.19$ in the self-similar region. Previous estimates of the lateral RMS velocity normalized by the mean centreline axial velocity were found to be equal to 0.25, 0.19 and 0.21 by Wygnanski and Fiedler (1969), Panchapakesan and Lumley (1993) and Hussein, Capp and George (1994), respectively. Only $w_{rms}/\langle U_{CL}\rangle$ compares well with the results of previous studies, as expected, given the previous research which indicates that the u- and v-components of the RMS velocity measured using ADV have abnormally high levels of noise.

The results presented in this section have validated the use of flying hot-film anemome-

try to estimate the mean and RMS velocities. The results also validate the use of ADV for the mean velocities (measured in all three directions) and the RMS velocity (measured in the z-direction, w_{rms}, *only*). In addition, ADV has shown itself to be more accurate than the flying hot-film anemometer at low velocities (far downstream and near the edges of the jet). Therefore, in the subsequent measurements herein, flying hot-film anemometry will be used for measurements of the mean and RMS axial velocities. On the other hand, ADV will be used to measure: i) the mean radial velocities, and ii) the mass flow rate and the half-width, which require especially accurate mean velocity measurements in the edges of, and far downstream in, the jet. In addition, the ADV (z-component) will be used along with the flying hot-film for the measurements of the RMS velocities in the background turbulence, as only one velocity component of this flow can be measured by the flying hot-film anemometer.

4. Results

4.1. *Turbulent background*

The random jet array produced a turbulent background flow that was approximately isotropic and with zero-mean flow. Figure 1 showed a schematic of the RJA, including the coordinate system used herein. A summary of the RJA performance is presented in Table 2. The statistics are presented at two "downstream" locations from the RJA ($y/M = 5.5$ and $y/M = 7.3$, where M is the mesh size, i.e., the distance between the jets, of the RJA). In this table, $\langle U \rangle$, $\langle V \rangle$, and $\langle W \rangle$ are the respective mean velocities in the horizontal transverse, downstream, and vertical transverse directions. u_{rms}, v_{rms} and w_{rms} are the RMS velocities in the same respective directions. S ($\equiv \langle u_\alpha^3 \rangle / \langle u_\alpha^2 \rangle^{3/2}$) and K ($\equiv \langle u_\alpha^4 \rangle / \langle u_\alpha^2 \rangle^2$) are the skewnesses and kurtoses of the velocity fluctuations ($u_\alpha = u$, v or w) in each direction. (Angular brackets denote average quantities.) The turbulent

kinetic energy per unit mass is defined as $\frac{1}{2}(\langle u^2\rangle+\langle v^2\rangle+\langle w^2\rangle)$. Due to the symmetry of the RJA, the statistics in the x and z directions should be identical. In Table 2, the statistics in the x-direction were measured with the flying hot-film anemometer. This is because the experimental setup only allows movement of the hot-film probe (and therefore measurements) in the x-direction. The statistics in the y- (downstream) and z-directions were measured using (the z-component of) the ADV.

The results for $\langle U_\alpha\rangle/u_{\alpha_{rms}}$ presented in Table 2 show that the zero-mean flow assumption is valid, and comparable to those of others (Variano *et al.* (2004) and Variano and Cowen (2008)). The small mean flow measured herein is also significantly lower than that generally found in quasi-isotropic turbulence generated by oscillating grids (up to 60%) (Fernando and De Silva, 1993; Thompson and Turner, 1975; McDougall, 1979).

For an isotropic flow, the ratios of the RMS velocities should be 1. The results in Table 2 indicate that the flow is close to being isotropic at the measurement locations (especially in the transverse plane). The flow generated by oscillating grids is typically characterized by anisotropy ratios between 1.1 and 1.2 (Hopfinger and Toly, 1976).

The observed $O(1)$ skewness of the fluctuating downstream velocity indicates that the probability density function (PDF) of v is asymmetric, with a greater chance of positive fluctuations than negative ones. This is a feature of spatially decaying turbulence (Maxey, 1987; Variano and Cowen, 2008). The skewnesses of the u and w velocity fluctuations, however, indicate that their PDFs are almost perfectly symmetric. The kurtosis of all velocity components are greater than 3, indicating that the probability of larger fluctuations is somewhat greater than that of a Gaussian distribution.

Eulerian temporal velocity spectra of the downstream and transverse velocity components (measured with the ADV at $y/M = 5.5$ and 7.3) are plotted in Figure 7(a). All three spectra are similar, each having a moderately large inertial subrange. The spectrum

of the downstream velocity component is also higher in the energy containing range (low frequencies) when compared to that of the transverse one, consistent with the larger RMS values given in Table 2 (shown only for $y/M = 7.3$). However, the spectra are similar in the inertial subrange and dissipation range.

Velocity spectra of the horizontal transverse (x) velocity component measured with the FHFA at $y/M = 5.5$ and 7.3 downstream of the RJA are plotted in Figure 7(b). In contrast with the Eulerian temporal spectra measured with the ADV and shown in Figure 7(a), the FHFA measured Eulerian spatial spectra that were calculated by taking the Fourier transform of the spatial autocorrelation ($\langle u(x)u(x+r)\rangle$). (However, for the latter to be two-point, one-time autocorrelations, the traversing velocity of the flying hot-film sensor must be significantly greater than the RMS velocity of the background flow (i.e., $u_{rms}/\langle U\rangle << 1$), akin to the requirement necessitated by Taylor's hypothesis when converting temporal measurements into spatial ones.) The FHFA spectra also exhibit a large separation of scales, as well as a spike at $\kappa_1 \approx 1{,}300$ m^{-1} (or f ≈ 20 Hz), which presumably results from a vibration in our traversing mechanism that we were unable to eliminate. Its contribution, however, is small as the area under the spike is $3{\times}10^{-4}\%$ of the total area under the spectrum (for $y/M = 7.3$), where the latter is proportional to the turbulent kinetic energy per unit mass of the flow. Furthermore, its origin does not derive from vortex-shedding from the probe support, as the Strouhal number of the spike, based on the chord of the airfoil support, is over 20 times larger than the value of ~ 0.2 observed for low-Reynolds-number airfoils at zero angle of attack.

The downstream decay of the background turbulence was determined by measuring the velocities along a transect orthogonal to the plane of the RJA, at different positions — i.e., different (x/M, z/M). Results are shown in Figure 8, which plots the downstream decay of the vertical transverse (w_{rms}, measured with the ADV) and the horizontal

transverse (u_{rms}, measured with the FHFA) RMS velocities. It is clear that, far enough away from the grid, the RMS velocities, and therefore turbulent kinetic energy, become independent of the transverse location, as the four curves collapse for $y/M > 6$. This implies that the turbulence becomes axisymmetric about the y-axis. In this region, a log-log version of this plot indicates that the RMS velocities measured with the ADV and the flying hot-film decay as $\sim y^{-1.31}$ and $\sim y^{-1.37}$, respectively – slightly faster than the y^{-1} dependence observed in oscillating grid turbulence.

Although the flow decays in the y-direction, the symmetric configuration of the random jet array should result in a two-dimensional flow (away from the boundaries and far enough downstream). Figure 8 has already provided evidence supporting this hypothesis. To further verify the flow's homogeneity in these directions, measurements of the turbulent background velocity field were acquired in vertical planes. The ADV measurements were conducted at $y/M = 7.3$, along four transects, two horizontal, which passed through: a) $z/M = 0$, and b) $z/M = 1.5$; and the other two vertical, which passed through: c) $x/M = 0$, and d) x/M = -1.5. (For the purposes of this discussion *only*, the coordinate system shown in figure 1 is now centred on the RJA, between 4 jets, in the plane of the jet exits.) The RMS vertical velocity fluctuation (w_{rms}, in cm/s) were measured every $0.25M$ over a $4M$ long interval in the horizontal and a $3M$ interval in the vertical, and are parameterized by their (average, standard deviation, minimum, maximum) values, as follows: a) (1.45, 0.031, 1.42, 1.52), b) (1.50, 0.045, 1.43, 1.60), c) (1.51, 0.38, 1.45, 1.56), and d) (1.52, 0.050, 1.44, 1.58). The reasonable degree of homogeneity was also confirmed by the FHFA measurements of u_{rms} performed along a $5M$-long horizontal transect, passing through $z/M = 0$, and conducted at $y/M = 5.5$ and $y/M = 7.3$. The respective results were (2.27, 0.14, 2.05, 2.54) and (1.56, 0.051, 1.46, 1.65). The flow is clearly not homogeneous in the y-direction due to the decay of the turbulence away from

the RJA. Consistent with Figure 8, the flow's homogeneity increases with downstream distance. (This decay could theoretically be reduced over a central part of the flow by the construction of a second RJA that would be placed in the tank facing the existing one. By symmetry, the two decaying flows would "cancel" one another, at least near the centre of the flow field, away from both RJAs. The magnitude of this hypothetical "homogenous core," however, is not clear and would be difficult to predict.) Lastly, we remark that an inhomogeneity of the background turbulence will exist across the jet in the y-direction. It, however, is small. Considering measurements made at $x/D = 50$ in a jet emitted into a turbulent background, the turbulence decays 5.3% across the jet half-width for the low turbulent kinetic energy background, and 7.7% in the case of the high turbulent kinetic energy background. We reiterate, however, that all radial profiles were measured in the vertical (z) direction, in which the background turbulence is homogeneous.

4.2. *Turbulent jet emitted into a turbulent background*

This subsection presents the main results of the current work: statistics of an axisymmetric turbulent jet issuing into a turbulent background with zero mean flow. Two different levels of turbulent kinetic energy (TKE $= \frac{1}{2}\langle u_i u_i \rangle$) of the background turbulence were considered: TKE = 4.44 cm^2/s^2 and 9.33 cm^2/s^2, corresponding to the two downstream distances presented in Table 2. In the rest of this subsection, these will be referred to as the low and high levels of TKE, respectively. Three jet Reynolds numbers are studied herein: 10,600, 5,800 and 5,300. The first was chosen since it was the highest one that could be reached in the present apparatus. Such a high Reynolds number jet did not breakup within the range of downstream distance accessible in our (relatively large) facility. Therefore, two lower Reynolds numbers were studied — one of which was rapidly destroyed by the background turbulence (Re = 5,300), while the other one (Re = 5,800)

was destroyed towards the end of our measurement region, permitting the jet breakdown to be more clearly observed.

Figure 9 plots the downstream evolution of the centreline mean axial velocity of a turbulent jet (normalized by the nozzle exit velocity) issuing into a quiescent flow and into the low and high levels of background turbulence for three jet Reynolds numbers. One observes that the background turbulence causes an accelerated decay of the jet centreline velocity. In the presence of background turbulence, i) the jet decays faster as the level of background turbulence increases, and ii) we observe that the jet decay is initially governed by a power-law. The decay constants (determined only from the power-law decay region) for the three Reynolds numbers are given in Table 3. The power-law region is then followed by a faster, quasi-logarithmic decay. In addition, the centreline mean velocity of the jet at the low level of background turbulence effectively reaches zero (defined as $\langle U \rangle / U_J \approx 0.01$) at downstream distances of $x/D = 90$, 60 and 45 for $Re = 10{,}600$, 5,800 and 5,300, respectively. The centreline mean velocity for the higher level TKE reaches zero earlier, at $x/D = 80$, 50 and 30 at the same respective Reynolds numbers. The point where the jet centreline velocity reaches zero is indicative of the location at which the jet's mean velocity field no longer "exists." Lastly, note that, for the case of a jet in the background turbulence at $Re = 5{,}300$, the measured mean velocities appear to fall to slightly negative values far downstream. This is most likely due to error from a minor drift in the hot-film calibration and/or inaccuracies related to the subtraction of the (moving) probe's translational velocity when dealing with these very low mean velocities of the jet.

The radial profile of mean axial velocity was next measured in quiescent and turbulent backgrounds. Radial profiles of the $Re = 10{,}600$ jet at $x/D = 20$, 30, 40 and 50 are shown in Figure 10. It can be seen that the ambient turbulence accelerates decay of the

jet, which exhibits lower mean velocities across the radial profile. Furthermore, the effect of the background turbulence becomes more noticeable farther downstream. Figure 11 shows the radial profiles of mean axial velocity for Re = 5,800. Beyond $x/D = 30$, the jet profile is distorted and relatively flat when in the presence of background turbulence, indicating that the organized jet structure has been destroyed. Radial profiles were not measured at Re = 5,300.

Figure 12 plots the radial profile of the mean radial velocity ($\langle V \rangle$) for the jet in quiescent and turbulent backgrounds. Radial profiles at x/D = 35, 42.5, 50, 60 and 75 are presented. Given the relatively small magnitude of the radial velocities ($\langle V(r) \rangle / \langle U_{CL} \rangle \approx 1/40$; Pope, 2000), the scatter in the results will be larger for velocity measurements of $\langle V(r) \rangle$. The measurements were conducted at Re = 10,600 using the ADV. In contrast to the mean axial velocities, the mean radial velocities increase in the presence of background turbulence (most notably closer to the edges of the jet). In addition, the jet is (relatively) wider in the presence of the background turbulence, as already observed for the mean axial velocity profile, and to be quantified below using the concept of jet half-width. The mean radial velocities at the edges of the jet in a quiescent background are negative. In the presence of background turbulence, the mean radial velocities remain negative at the edges, but the negative velocity regions (presumably) cannot be seen in the profiles for $x/D \geqslant 50$ as the measurements were only conducted up to $r/x = 0.3$ (which was not far enough in the radial direction). Negative radial velocities at the edges of the jet in the presence of background turbulence are indicative of fluid being entrained into the jet. Therefore, a concurrent increase in the mass flow rate with the downstream distance would also be expected in the presence of the background turbulence, as will be discussed shortly. In addition, the radial velocities close to the centreline do not significantly change in the presence of background turbulence, in contrast with the radial

velocities away from the centreline which clearly increase. Furthermore, the difference between the radial velocities at the edges of the jet in the presence of background turbulence and the radial velocities at the edges of the jet in the quiescent background increases from $x/D = 35$ to $x/D = 75$ — the high-TKE background results in larger radial velocities, especially close to the edges of the jet, when compared to the low-TKE background. Lastly, we note that agreement between the radial velocities measured by the ADV and those inferred from the measurements of $\langle U \rangle$ and the continuity equation (not shown) are of a comparable quality to those calculated for the jet emitted into a quiescent background.

The downstream evolution of the half-width of the jet in quiescent and turbulent backgrounds is shown in Figure 13. The measurements were conducted at $Re = 10{,}600$ using the ADV. The solid and dashed horizontal lines in these graphs correspond to the integral length scales of the background turbulence for the low- and high-TKE cases, respectively. The jet in a quiescent background grows linearly with downstream distance, as predicted. However, in the presence of background turbulence, the jet becomes wider as the level of background turbulence increases. Furthermore, the evolution of the jet half-width in the presence of external turbulence is no longer linear and exhibits power-law growth $\sim x^{1.5}$ and $\sim x^{1.7}$ for the low- and high-TKE backgrounds, respectively. The length scale of the jet is smaller than that of the background turbulence for most downstream positions. The effect of the length scale of the background turbulence on the jet is presumably more noticeable closer to the jet exit, and reduces with increasing downstream distance.

As mentioned earlier, the presence of background turbulence decreases the mean axial velocity of the jet. If entrainment is proportional to the characteristic velocity of the jet (Morton *et al.* 1956), then a decrease in centreline velocity would imply a decrease in the

rate of entrainment. Applying this argument to the present results implies that ambient turbulence should result in a decrease in the (near-field) jet entrainment. This is verified by calculating the mass flow rate of the jets (using the radial profiles of axial velocity).

Mass flow rates were calculated by integrating the area under the mean velocity profiles (and assuming axisymmetry). The downstream evolutions of the mass flow rates (normalized by the mass flow rate at the nozzle exit, m_0), measured in quiescent and turbulent backgrounds by ADV, are plotted in Figure 14. One observes that background turbulence serves to decrease the mass flow rate of the jet (at a given downstream distance), from which it can be inferred that the entrainment is also reduced. This suggests that the background turbulence may break up the large-scale structure of the jet.

The measured jet entrainment rate (i.e., dm/dx) in a quiescent background is 0.34. In the presence of background turbulence, our experiments indicate that the entrainment rate of the jet remains constant for a given level of background turbulence for the finite downstream distances studied herein (i.e., m is a linear function of x). However, the entrainment rate in the presence of background turbulence is lower than that in a quiescent background, and its magnitude appears to decrease with increasing intensity of the background turbulence — the rate of entrainment decreasing from 0.19 (in the low-TKE background) to 0.16 (in the high-TKE background). Given that the mass flow rate is proportional to $r_{1/2}^2\langle U_{CL}\rangle$, m must be proportional to x for a jet in a quiescent background. The fact that we observe the same to hold for the jets emitted into a turbulent background is noteworthy, if not wholly unexpected. Because i) $r_{1/2} \propto x^{1.5}$ ($\propto x^{1.7}$), and ii) $\langle U_{CL}\rangle \propto x^{-1.83}$ (or $\propto x^{-2.13}$) for the $Re = 10,600$ jet emitted into the low (or high) TKE backgrounds, the predicted power-law exponent for the downstream evolution of m should be $2 \times 1.5 - 1.83 = 1.17$ (or $2 \times 1.7 - 2.13 = 1.27$). Whether the difference in the exponents from 1 is physically significant is difficult to ascertain. The difference in the

fit of a power law ($m/m_0 = A(x/D)^n$) and a linear function ($m/m_0 = A \times (x/D) + B$) in negligible.

Given the previously discussed power-law evolutions of $\langle U_{CL} \rangle$ and $r_{1/2}$ of the jet emitted into a turbulent background, one notes that the momentum integral for the jet ($M \equiv \int_0^\infty 2\pi r \rho \langle U \rangle^2 dr \propto r_{1/2}^2 \langle U_{CL} \rangle^2$) is no longer constant and decreases, unlike that for a jet in a quiescent background. We emphasize that this is not a violation of the principle of conservation of momentum, but rather an indication that the assumptions (involved in the analysis leading to the conclusion that M is independent of x for a jet in a quiescent background) no longer hold in the case where the background is turbulent.

Lastly, it is worth mentioning that the effect of a turbulent background on the mass flow rate of a jet is observed farther upstream when the turbulent kinetic energy of the background flow is increased. At $x/D = 35$, the values of m/m_0 for the quiescent background and the low-TKE background are similar, whereas m/m_0 for the high-TKE background is already much smaller than that observed for a jet in a quiescent background (at the same downstream position). We hypothesize that the effects of the background turbulence on the jet are most significant when the RMS velocities of the background turbulence are larger than the RMS velocities of the jet.

The effect of background turbulence on the RMS axial velocities of the jet at *Re* = 10,600, 5,800 and 5,300 when issued in two different turbulence levels is shown in Figure 15. The solid and dashed horizontal lines in these graphs correspond to the RMS velocity of the background turbulence for the low- and high-TKE cases, respectively. It is expected that the effect of background turbulence on the jet should be a function of the relative magnitude of the i) RMS velocities, and ii) integral length scales, of the jet and background turbulence. These results show that the RMS axial velocity of the jet increases in the presence of a turbulent background. Moreover, the effect of external

turbulence seems to be higher near the jet exit (i.e., the percentage difference between the RMS velocity of the jet in the quiescent and turbulent backgrounds decreases with the downstream distance). As was shown earlier, the integral length scale of the jet close to the jet exit, i.e., $x/D \leqslant 35$, is less than that of the background turbulence, but grows larger with downstream distance. Therefore, the RMS velocity field may be more strongly affected near the jet exit where the integral length scale of the jet is lower than (or similar to) that of the background turbulence. Furthermore, the RMS velocities of the jet in the high-TKE background are higher compared to those of the jet in low-TKE background close to the jet exit, *i.e.*, $x/D \leqslant 35$ for $Re = 10{,}600$, and $x/D \leqslant 15$ for $Re = 5{,}800$ and 5,300. This trend changes in the near-field (after the initial development region of the jet) where the RMS velocities of the jet in the low-TKE background are higher than those of the high-TKE background, i.e., $40 \leqslant x/D \leqslant 100$ for $Re = 10{,}600$, and $20 \leqslant x/D \leqslant 45$ for $Re = 5{,}800$ and 5,300. This is in contrast with the notion of superposition of the jet and background turbulence. Finally, far downstream (where the measured RMS velocities are close to those of the background turbulence), the RMS velocities of the jet in the high-TKE background are higher than those of the low-TKE background, as would be expected. When the RMS velocities of the jet are equal to those of the background turbulence, one could argue that the jet no longer "exists" and is completely "destroyed," since both its mean and fluctuating velocity fields can no longer be observed. Furthermore, it can be seen that the RMS velocities decrease to background turbulence levels at locations farther downstream than those where the mean velocity reached zero (discussed earlier). Given that the jet RMS velocity field "outlasts" its mean velocity field, one could infer that what remains is a volume of turbulent flow with no mean velocity and therefore no jet structure, once the mean velocity field "disappeared." As can be seen in Figure 15(a), the jet is not

totally destroyed by the background turbulence within the measurement range for the higher Reynolds number jet. However, at lower Reynolds numbers, the RMS velocities asymptote to the RMS velocities of the background turbulence, indicating that the latter destroyed the jet within the measurement range.

Figures 16 and 17 show the radial profiles of the RMS axial velocity of the jet in quiescent and turbulent backgrounds at Re = 10,600 and Re = 5,800, respectively, at downstream distances of x/D = 20, 30, 40 and 50. It can be seen that the axial RMS velocities increase in the presence of background turbulence, albeit not always proportional to the intensity of the latter. In particular, the RMS velocities of the jet issued into the high-TKE background are higher than those of the jet in the low-TKE flow, for $x/D \leqslant 35$ for Re = 10,600 and $x/D \leqslant 15$ for Re = 5,800 (not shown) and at the edges of the jet (where the background turbulence is dominant). Downstream of these initial regions, the RMS velocities of the jet are higher for the low-TKE background. Finally, when the jet structure is disrupted and the external turbulence is dominant, *e.g.*, $x/D \geqslant 50$ for Re = 5,800, the RMS velocities measured in jet in high-TKE are higher.

A typical profile of the local turbulence intensity ($u_{rms}/\langle U(r)\rangle$, measured at x/D = 30 for Re = 10,600) is plotted in Figure 18. The turbulence intensities increase in the presence of background turbulence (as expected given the lower mean axial velocities and higher RMS axial velocities presented earlier). Furthermore, the turbulence intensities of both quiescent and turbulent backgrounds increase from the centreline toward the edge of the jet, as does the difference in turbulence intensities between a jet released into a quiescent background, and one released into a turbulent one.

5. Discussion

The purpose of this section is to discuss and interpret the results just presented. In particular, the question of i) self-similarity of the jet in a turbulent background, ii) entrainment mechanisms in the presence of background turbulence, iii) a parameterization of the breakup location of the jet, and iv) the interfacial region between the jet and the turbulent environment will be addressed.

5.1. *The question of self-similarity of a jet in a turbulent background*

The axisymmetric turbulent jet, when i) emitted into a quiescent background, and ii) for sufficiently large downstream distances, is nominally self-similar. (The reader is referred to George (1989) or Hussein, Capp and George (1994) for more details pertaining to the issues of initial-condition-dependence and the effects of non-infinite environments.) However, the previous results clearly indicate that the jet emitted into a turbulent background is not self-similar as plots of $\langle U \rangle / \langle U_{CL} \rangle$ vs. $r/r_{1/2}$ (not shown) do not collapse for different downstream distances nor different levels of background turbulence. Furthermore, the downstream evolution of the local turbulence intensity on the jet axis (i.e., plots of $u_{rms-CL}/\langle U_{CL} \rangle$ vs. x/D) cannot asymptote to a constant value, but tends to infinity (since for large x/D, u_{rms-CL} tends to the constant value of the background turbulence, whereas $\langle U_{CL} \rangle$ tends to zero). The multiplicity of both velocity and length scales in a jet emitted into a turbulent background precludes the existence of a self-similar behaviour.

5.2. *Entrainment mechanism*

The lack of self-similarity of a jet issuing into a turbulent background indicates a change in the jet's structure, which would modify its entrainment mechanism. Here, we hypothesize how the entrainment is affected by the background turbulence.

As shown in §4.2, the background turbulence results in: i) an increase in both the

(large-scale) turbulent length and velocity scales, as inferred from measurements of the half-width and RMS velocity, ii) a decrease in the mean axial velocity of the jet, iii) a faster decay rate of the centreline mean axial velocity, and iv) a reduced rate of increase in the mass flow rate of the jet, (i.e., a decrease in the jet entrainment rate). These phenomena are consistent with the background turbulence reducing the entrainment by engulfment by modifications to the large-scale structure of the jet.

However, background turbulence also affects the jet's boundary, thus disrupting entrainment by nibbling. For the case of the jet issuing into a quiescent background, Westerweel *et al.* (2009) detected discontinuities in quantities such as the conditional momentum flux and the (mean and fluctuating) vorticity at the laminar superlayer. Such a discontinuity presumably vanishes when the background turbulence is present, as these quantities asymptote to that of the background turbulence instead of rapidly dropping to zero. Therefore, simple gradient transport arguments would suggest that the flux of vorticity into the background turbulence should decrease (compared to that in a quiescent background) due to a lower gradient at the interface. It is therefore hypothesized that, entrainment by nibbling (resulting from diffusion of vorticity) is also reduced in the presence of background turbulence.

Furthermore, the entrainment mechanism for the jet may change in the presence of background turbulence. No discontinuity was observed by Westerweel *et al.* (2009) in RMS conditional velocities and the integral length scale which "exist" (i.e., are finite, non-zero and measurable) on both sides of the jet/background interface, but these quantities tend to zero in the quiescent fluid. However, in the presence of the background turbulence, eddies with (RMS) velocities and length scale on the order of those of the background turbulence dominate at the interface. Consequently, entrainment by viscous diffusion at the interface (or laminar super-layer) is changed to turbulent diffusion by large-scale

eddies in the presence of external turbulence. If (in the presence of the background turbulence) nibbling by small-scale eddies at the jet/background interface were the main entrainment mechanism, then the mass flow rate of the jet should have decreased, or at least not increased, with downstream distance. The observed, persistent increase of the mass flow rate of the jet issuing into a turbulent background with the downstream distance indicates that the entrainment may occur via large-scales / engulfment, or by a third mechanism, such as turbulent diffusion. The latter is consistent with the notion of an increased effective eddy viscosity in the turbulent background. In the case of a jet emitted into a quiescent background, Westerweel *et al.* (2005) demonstrated that the effective eddy viscosity, defined in *laboratory* coordinates, decreased from its value just inside the turbulent/non-turbulent interface to a smaller, but finite, non-zero value outside the shear layer. Thus, in the case of a jet emitted into a turbulent background, where the eddy viscosity is clearly non-zero outside of the jet (independent of the coordinates), it stands to reason that turbulent diffusion will be enhanced. This effect bears many similarities with what occurs in so-called shearless mixing layers (to be discussed in §5.4). However, drawing solid conclusions regarding the entrainment mechanism of the jet in the presence of background turbulence – solely from the velocity field – is not easy, and information pertaining to the mixing of scalars within the jet would be of further benefit.

5.3. *Breakup location of the jet*

It can be argued that if the turbulent Reynolds number of the background turbulence were much larger than that of the jet, the jet structure would break up upon its arrival into the background flow. However, if the converse was true, it would be reasonable to expect that the jet would develop downstream and its structure would be similar to a jet issuing into a quiescent background (where the Reynolds number of the surroundings is zero). Here, we study the breakup location of the jet as a function of both the jet and

background turbulence parameters, which are expected to be a function of i) the RMS velocities of both the background turbulence and that of the jet, ii) the integral length scales of both the background turbulence and that of the jet, and iii) their respective turbulent Reynolds numbers, which are obviously related to u_{rms} and ℓ, as well. However, note that the turbulent jet Reynolds number (e.g., $Re_{Jet} = u_{rms-Jet}\ell_{Jet}/\nu$, where ℓ_{Jet} is the integral length scale of the jet emitted into a turbulent background) of the jet is not constant. (Nor would be the Taylor-microscale Reynolds number.) Consequently, there is no obvious choice of a turbulent Reynolds number to characterize the jet. Because i) $u_{rms-Jet} \propto U_{CL} \propto U_J$, and ii) $\ell_{Jet} \propto D$, the overall Reynolds number of the jet ($Re = U_J D/\nu$) is used as a surrogate for the turbulent Reynolds number of the jet. Therefore, we define $Re_{T-RJA}/Re_{Jet} = u_{rms-RJA}\ell_{RJA}/U_J D$, which can be interpreted as the relative magnitude of the turbulent Reynolds number of the background turbulence to the jet Reynolds number. Quantifying the jet Reynolds number in terms of parameters known *a priori* therefore allows the prediction of the jet breakup location, which is of relevance to practical applications, such as the release of (a jet of) sewage into the ocean, etc.

The breakup location herein is determined from the centreline mean velocity and is defined as the position where the mean axial velocity reaches 1% of the exit velocity of the jet. Figure 19 plots the breakup location of the jet (found using the mean axial velocity measurements in §4.2) as a function of Re_{T-RJA}/Re_{Jet}. The data points on this graph correspond to the three different jet Reynolds numbers of 10,600, 5,800 and 5,300 issuing into turbulent backgrounds with TKE = 4.44 $\mathrm{cm}^2/\mathrm{s}^2$ and 9.33 $\mathrm{cm}^2/\mathrm{s}^2$. As seen in this graph, the breakup location is a decreasing function of Re_{T-RJA}/Re_{Jet}, albeit with some scatter. Extrapolation of the results predicts that at higher Re_{T-RJA}/Re_{Jet} (~ 0.4), the jet breaks up at its exit ($x/D = 0$). Lastly, we remark that a breakup location based on

the centreline RMS velocity did not exhibit any clear dependence on Re_{T-RJA}/Re_{Jet}, as was the case for the mean velocity field.

The decay exponent (of the power-law decay region) of the centreline mean velocity of the jet is also plotted versus Re_{T-RJA}/Re_{Jet} in Figure 19 and is a decreasing function of Re_{T-RJA}/Re_{Jet}, again indicating that the jet decays faster as the background turbulence increases and/or the jet Reynolds number decreases. We note that the most negative decay exponent in this graph ($m \approx$ -4.3) was for the lowest Reynolds number jet ($Re = 5,300$) in the high-TKE background and may not be accurate as it was determined from only (the first) three data points, as the jet mean velocity had decreased to zero beyond that downstream distance.

5.4. *Interfacial region between the jet and the turbulent environment*

We finish the discussion by analyzing the interfacial region between the jet and the turbulent environment both quantitatively, using so-called "Phillips theory" (Phillips 1955; see also, for example, Fabris, 1979; Gharbi, Amielh and Anselmet, 1995), and qualitatively by relating our results to those observed in shearless mixing layers (e.g., Veeravalli and Warhaft, 1989; Tordella and Iovieno, 2006).

Phillips (1955) developed theoretical arguments to investigate the structure of the interfacial region between a turbulent and quiescent fluid and made two predictions. The first was that the variances of the three components of the velocity fluctuations in the irrotational region outside a free turbulent boundary should be inversely proportional to the fourth power of the distance from the jet axis (r). (Applying the analysis for a jet in a turbulent background and comparing it to the results in a quiescent background, can provide insight into behaviour of the interfacial region.) The second prediction, for which we do not have the data to verify, was that the variance of the velocity fluctuation normal to the interface should be equal to the sum of the variance of the other two components.

Figure 20 plots $u_{rms}^{-1/2}(r)$, normalized by its centreline value, as a function of $r/r_{1/2}$ for an $Re = 10,600$ jet emitted into quiescent and turbulent backgrounds. Phillips's first prediction is verified if the data are proportional to r. According to Gharbi et al. (1995), there are three main regions in a jet. The first is the central core of the jet. It is a non-intermittent region starting from the centerline and extending to $r/r_{1/2} \sim 1$, in which the normalized RMS velocities undergo a small evolution and remain approximately equal to 1. The second region separates the central core of the turbulent flow from the ambient flow (which, we note, is a co-flow in the case of Gharbi et al. (1995)). In this intermittent, interfacial region, the normalized RMS velocities exhibit substantial variations. For $2 \lesssim r/r_{1/2} \lesssim 3$, Gharbi et al. (1995) observed $u_{rms}^{-1/2}(r)/u_{rms}^{-1/2}(0) \propto r/r_{1/2}$, in accordance with Phillips' first prediction. In the third region, the RMS velocities asymptote to the values of the surroundings.

Figure 20 indicates that the jet in a quiescent background has $u_{rms}^{-1/2}(r)/u_{rms}^{-1/2}(0) \approx 1$ in the core of the jet, as expected. This value increases linearly, according to the Phillips's first prediction for $1.5 \lesssim r/r_{1/2} \lesssim 2.5$. Close to the edges of the jet ($r/r_{1/2} \geqslant 4$), the RMS velocities reach a plateau. For the case of the jet in the presence of background turbulence, the RMS velocities similarly exhibit a small dependence on r in the central core. The linear region still exists, although its slope is lower than that in a quiescent background and decreases with increasing x/D, due to the reduction in the difference between $u_{rms}(0)$ and $u_{rms}(r \to \infty) = u_{rms-RJA}$. Furthermore, as the jet develops downstream, the second region moves towards the jet centerline, reducing the extent of the jet's central core of constant RMS velocity. At $x/D = 50$, the linear region appears to start from the jet centreline, due to the disappearance of the first region. At this point, the background turbulence has "penetrated" the entire jet.

The interfacial, outer regions of a jet emitted into background turbulence also resemble

what are called shearless mixing layers (e.g., Veeravalli and Warhaft, 1989; Tordella and Iovieno, 2006). These are (inhomogeneous) flows with no difference in mean velocities, but comprised of two layers with differences in their turbulent fields (i.e., integral length scale, turbulent kinetic energy). Previous (experimental and numerical) research parameterized the flows by means of the ratios of the integral length scales ($\mathcal{L}$) and turbulent kinetic energies ($\mathcal{E}$) in each layer. Veeravalli and Warhaft (1989) experimentally found that when $\mathcal{L} \sim 1$, the flow is characterized by a unique scale, and a region of high turbulent kinetic energy (TKE) diffuses into a region of low TKE. In the limit where $\mathcal{L}$ is significantly different than one, they argued that the flow is dominated by its large-scale side (which is also their large TKE side). For intermediate values of $\mathcal{L}$, they found both scales play a significant role in the energetics. Tordella and Iovieno (2006), who numerically simulated a shearless mixing layer, found that the intermittency and the depth-of-penetration of the eddies from the high-TKE layer increased when the energy and length scale gradients are concordant (i.e., both $\mathcal{L}$ and $\mathcal{E}$ are > 1 or both $\mathcal{L}$ and $\mathcal{E}$ are < 1), and decrease when they are opposite (i.e, $\mathcal{L} > 1$ and $\mathcal{E} < 1$, or vice-versa). Tordella, Iovieno and Bailey (2008) simulated a shearless mixing layer with $\mathcal{L} = 1$, to solely study the effect of $\mathcal{E}$, finding that intermittency still arose, indicating that the presence of a TKE gradient is the minimal requirement to observe a departure from Gaussianity in the mixing layer. Tordella and Iovieno (2012) subsequently examined a shearless mixing layer in which $\mathcal{E} = 1$, observing a nonlinear interaction in which the inhomogeneity in length scales could induce inhomogeneity in the TKE due to the more rapid decay of TKE associated with the smaller-scale region.

For a jet emitted into a turbulent background, both $\mathcal{L}$ and $\mathcal{E}$ are relevant parameters as both vary with downstream distance in the jet. Defining $\mathcal{L} \equiv \ell_{jet}/\ell_{background}$ and $\mathcal{E} \equiv \frac{1}{2}\langle u_i u_i \rangle_{jet}/\frac{1}{2}\langle u_i u_i \rangle_{background}$, one notes that $\mathcal{L}$ is an increasing function of x/D,

whereas $\mathcal{E}$ is a deceasing function of x/D. In the present work, $\mathcal{L} < 1$ and $\mathcal{E} > 1$ for most values of x/D. However, in the limit of large x/D, $\mathcal{L} \gtrsim 1$ and $\mathcal{E} \to 1$. Therefore, the case of $\mathcal{L} \sim 1$, which has been of particular interest to those who have studied shearless mixing layers, is nothing more than an intermediate, transient situation that only occurs at a certain value of x/D for the values of D and $\ell_{background}$ employed herein. However, this comparison further emphasizes the role of the relative length scales of the two flows, in addition to that of the RMS velocities, as was discussed for the breakup location of the jet, which was parameterized as a ratio of Reynolds numbers, but that could have also been reexpressed as $1/(\mathcal{L}\mathcal{E}^{1/2})$.

At the measurement locations closet to the jet exit, where $\mathcal{L} \ll 1$ and $\mathcal{E} \gg 1$, the results of Tordella and Iovieno (2006) imply that the intermittency and the depth-of-penetration of the eddies from the high-TKE layer decrease. This may appear to be in contradiction with the values of u_{rms} at small x/D, measured on the axis of the jet emitted into a turbulent background (see Figure 15), which significantly exceed those obtained by (naively) adding the turbulent kinetic energies of the jet and the surrounding background (i.e., $u_{rms\,simple\,superposition} = [u^2_{rms\,quiescent\,jet} + u^2_{rms\,RJA}]^{1/2}$). This can be explained by the differences between a jet emitted into a turbulent flow and a shearless mixing layer. Whereas the simulated shearless mixing layer is homogeneous in the direction parallel to the interface between the two layers, this is not the case for a jet emitted into a turbulent environment, and especially not in the immediate vicinity of the jet exit. At the exit, the Kelvin-Helmoltz instability that engenders fully turbulent flow farther downstream will be modified by the background turbulence. There, the background turbulence is of a larger length scale that of the jet, which may not have as large of a turbulence intensity as it exhibits slightly farther downstream, where our first measurements were made. The interaction of the background turbulence and the jet in its initial flow development

region presumably results in a significant amplification of the turbulence intensity farther downstream. (This, however, is best confirmed by measurements of a scalar emitted by a jet in a turbulent background, given that the presence of a background turbulence no longer renders it possible to differentiate when one measures inside and outside of the jet.) We also note that a similar large increase in the turbulence intensity was observed by Tsai *et al.* (2007) in wall jets emitted into turbulent backgrounds generated by an oscillating grid. As expected, they observed increased values of u_{rms} in the outer region of their wall jet. However, they also observed large increases in u_{rms} (as large as a factor of 2 – see their Figure 9) close to the wall, akin to what is observed herein in Figure 15. Their observed increases were also much larger than those that would be obtained by summing the turbulent kinetic energies of the turbulent background and that of the wall jet in a quiescent background. Tsai *et al.* (2007) also performed flow visualizations, which showed that the effect of the external turbulence was noticeable across the wall jet, causing significant changes in its structure.

6. Conclusions

The effect of different levels of background turbulence on an axisymmetric turbulent jet at various Reynolds numbers was investigated. To our knowledge, this is the first work to systematically study the effect of (quasi-)homogeneous turbulence on a turbulent jet. In the limited previous studies of the effect of background turbulence on a jet, the jet axis was in the direction of (significant) inhomogeneity in the flow, resulting in differing levels of background turbulence at different downstream locations in the jet.

The results show that the presence of background turbulence can have very significant effects on the evolution of a jet when compared to that in a quiescent environment. In particular, the mean axial velocity of the jet is reduced in the presence of background

turbulence. Furthermore, the decay rate of the mean axial velocity, which initially follows a power-law, then accelerates by becoming quasi-logarithmic, is increased in a turbulent environment. The observed mean velocity profiles are no longer self-similar in the presence of background turbulence.

It is shown that the background turbulence results in an increase in the mean radial velocities, as also confirmed by the observed increase in jet half-widths in the presence of background turbulence. Although the jet becomes wider, this effect is offset by the proportionally larger decrease in the mean axial velocities such that the jet mass flow rates, as well as its entrainment rate, are lower in the presence of background turbulence when compared to that in a quiescent environment. These latter results are consistent with i) the hypothesis of Hunt (1994) that predicted that external turbulence would serve to break up the jet and decrease its entrainment rate, and ii) the experimental study of Gaskin *et al.* (2004), who observed a decreased entrainment in a plane jet issuing into a shallow co-flow. The present study also showed that the entrainment mechanism most likely changes in the presence of background turbulence. As i) the interface between the jet and ambient flow is dominated by eddies of characteristic size on the order of that of the background turbulence, and ii) the vorticity gradient at the interface between the jet and background flow is significantly reduced, entrainment is most likely not due to the viscous diffusion of vorticity / nibbling, as is the case for a jet in a quiescent background (Mathew and Basu, 2002; Westerweel *et al.*, 2009), but could instead be related to turbulent diffusion.

The RMS axial velocities (u_{rms}) are found to increase in the presence of background turbulence, and asymptote to those of the surroundings farther downstream than the location at which the mean velocity falls to 1% of its value at the jet exit. Furthermore, a non-monotonic dependence of $u_{rms}(r)$ the on the level of the background turbulence is

observed and attributed to the varying contributions of turbulent production that results from the different decay rates of the mean axial velocities at different radial locations.

Lastly, the present work also quantified the break up location of the jet, as well as the decay rate of mean axial centreline velocity, as a function of the level of the background turbulence. The break up position (as determined from the mean velocity field of the jet) and the power-law decay exponent of the centreline velocity were found to be decreasing functions of the ratio of the turbulent Reynolds number of the background turbulence to the jet Reynolds number. Further studies that vary the length scales of the two turbulence fields, however, are recommended.

Acknowledgements

We would like to acknowledge the funding provided by the Natural Sciences and Engineering Research Council of Canada and the Fonds québécois de la recherche sur la nature et les technologies. We thank John Bartczak for his thoughtful suggestions and assistance during the design and construction of the apparatus. We also thank Marek Przykorski, who helped us with various electrical and electronic aspects of our experiments. Lastly, we acknowledge Jason Lepore and Arpi Berajeklian for their kind assistance with the hot-film anemometry measurements.

REFERENCES

Brown, G. L. & Roshko, A. 1974 Large scales in the developing mixing layer. *Journal of Fluid Mechanics*, 64, 775-816.

Ching, C. Y., Fernando, H. J. S. & Robles, A. 1995 Break down of line plumes in turbulent environments. *Journal of Geophysical Research*, 100 (C3), 4707-4713.

Corsin S. & Kistler A. L. 1955 Free-stream boundaries of turbulent flows. NACA Report No. 1244.

Cuthbertson, A. J. S., Malcangio, D., Davies, P. A. & Mossa, M. 2006 The influence of a localized region on turbulence on the structural development of a turbulent, round, buoyant jet. *Fluid Dynamics Research*, 38, 683-698.

Dahm, W. J. A. & Dimotakis, P. E. 1987 Measurements of entrainment and mixing in turbulent jets. *AIAA Journal*, 25, 1216-1223.

Dahm, W. J. A. & Dimotakis, P. E. 1990 Mixing at large Schmidt number in the self-similar far field of turbulent jets. *Journal of Fluid Mechanics*, 217, 299-330.

Dimotakis, P. E. 2000 The mixing transition in turbulent flows. *Journal of Fluid Mechanics*, 409, 69-98.

Fabris, G. 1979 Conditional sampling study of the turbulent wake of a cylinder. Part 1. *Journal of Fluid Mechanics*, 94(4), 673-709.

Ferdman, E., tgen, M. V. & Kim, S. 2000 Effect of Initial Velocity Profile on the Development of Round Jets. *Journal of Propulsion Power*, 16, 676-686.

Fernando, H. J. S. & De Silva, I. P. D. 1993 Note on secondary flows in oscillating-grid, mixing-box experiments. *Physics of Fluids*, A5 (7), 1849-1851.

Gaskin, S., McKernan, M & Xue, F. 2004 The effect of background turbulence on jet entrainment: an experimental study of a plane jet in a shallow coflow. *Journal of Hydraulic Research*, 42(5), 531-540.

George, W. K. 1989 The self preservation of turbulent flows and its relation to initial conditions and coherent structures. *Advances in Turbulence (ed. W.K. George & R.E.A. Arndt)*, 39-72. Hemisphere.

Gharbi, A., Amielh, M. & Anselmet. F. 1995 Experimental investigation of turbulence properties in the interface region of variable density jets. *Physics of Fluids*, 7, 2444-2454.

Guo, Y., Davies, P. A., Fernando, H. J. S. & Ching, C. Y. 1999 Influence of background turbulence on the evolution of turbulent jets. *Conference Proceedings of the 28th IAHR Congress.*

Guo, Y., Malcangio, D., Davies, P. A. & Fernando, H. J. S. 2005 A laboratory investigation into the influence of a localized region on turbulence on the evolution of a round turbulent jet. *Fluid Dynamics Research*, 36, 78-89.

Hopfinger, E. J. & Toly, J. A. 1976 Spatially decaying turbulence and its relation to mixing across density interfaces. *Journal of Fluid Mechanics*, 78, 155-175.

Hunt, J. C. R. 1994 Atmospheric jets and plumes. *In: Davies, P.A. and Valente Neves, M.I. (eds.), Recent Research Advances in the Fluid Mechanics of Turbulent Jets and Plumes, NATO ASI Series E*, 255, 309-334.

Hurther, D. & Lemmin, U., 2008 Improved turbulence profiling with field-adapted acoustic Doppler velocimeters using a bifrequency Doppler noise suppression method. *Journal of Atmospheric and Oceanic Technology*, 25(3), 452-463.

Hussein, H. J., Capp, S. P. & George, W. K. 1994 Velocity-measurements in a high-Reynolds-number, momentum-conserving, axisymmetrical, turbulent jet. *Journal of Fluid Mechanics*, 258, 31-75.

Khorsandi, B. 2011 Effect of background turbulence on an axisymmetric turbulent jet. PhD dissertation, McGill University.

Khorsandi, B., Mydlarski, L. & Gaskin, S. 2012 Noise in turbulence measurements using acoustic Doppler velocimetry. *Journal of Hydraulic Engineering*, 138(10), 829838.

Law, A. W. K., Cheng, N. S. & Davidson, M. J. 2001 Jet spreading in oscillating-grid turbulence. *Proceedings of the 3rd International Symposium on Environmental Hydraulics*, 1-6.

Lavertu, T.M., Mydlarski, L. & Gaskin, S.J. 2008 Differential diffusion of high-Schmidt-number passive scalars in a turbulent jet. *Journal of Fluid Mechanics*, 612, 439475.

Mathew, J. & Basu, A. 2002 Some characteristics of entrainment at a cylindrical turbulence boundary. *Physics of Fluids*, 14, 2065-2072.

Maxey, M. R. 1987 The velocity skewness measured in grid turbulence. *Physics of Fluids*, 30, 935-939.

McDougall, T. J. 1979 Measurements of turbulence in a zero-mean shear mixed layer. *Journal of Fluid Mechanics*, 94 (3), 409-431.

Morton, B. R., Taylor, G. I. & Turner, J. S. 1956 Turbulent gravitational convection from maintained and instantaneous sources. *Proceedings of the Royal Society, London*, Series A, 234: 1-23.

Mydlarski, L. & Warhaft, Z., 1996 On the onset of high-Reynolds-number grid-generated wind tunnel turbulence. *Journal of Fluid Mechanics*, 320, 331-368.

Nikora, V. I. & Goring, D. G. 1998 ADV measurements of turbulence: Can we improve their interpretation? *Journal of Hydraulic Engineering*, 124(6), 630-634.

Panchapakesan, N. R. & Lumley, J. L. 1993 Turbulence measurements in axisymmetric jets of air and helium. Part 1. Air jet. *Journal of Fluid Mechanics*, 246, 197-223.

Phillips, O.M. 1955 The irrotational motion outside a free turbulent boundary. *Mathematical Proceedings of the Cambridge Philosophical Society*, 51, 220-229

Pope, S. B. 2000 *Turbulent Flow*. Cambridge University Press.

Ricou, F. P. & Spalding, D. B. 1961 Measurements of entrainment by axisymmetrical turbulent jets. *Journal of Fluid Mechanics*, 11, 21-32.

Thompson, S. & Turner, J. S. 1975 Mixing across an interface due to turbulence generated by an oscillating grid. *Journal of Fluid Mechanics*, 67, 349-368.

Tordella, D. & Iovieno, M. 2006 Numerical experiments on the intermediate asymptotics of shear-free turbulent transport and diffusion. *Journal of Fluid Mechanics*, 549, 429-441.

Tordella, D. Iovieno, M. & Bailey, P.R. 2008 Sufficient condition for Gaussian departure in turbulence. *Physical Review E*, 77, 016309-1 - 016309-10.

Tordella, D. & Iovieno, M. 2012 Decaying turbulence: What happens when the correlation length varies spatially in two adjacent zones. *Physica D*, 241, 178-185.

Townsend, A. A. 1956 *The Structure of Turbulent Shear Flow*. Cambridge University Press.

Tsai, Y.S., Hunt, J.C.R., Nieuwstadt, F.T.M., Westerweel, J. & Gunasekaran, B.P.N. 2007 Effect of Strong External Turbulence on a Wall Jet Boundary Layer. *Flow Turbulence and Combustion*, 79, 155-174.

Variano, E. A., Bodenschatz, E. & Cowen, E. A. 2004 A random synthetic jet array driven turbulence tank. *Experiments in Fluids*, 37, 613-615.

Variano, E. A. & Cowen, E. A. 2008 A random-jet-stirred turbulence tank. *Journal of Fluid Mechanics*, 604, 1-32.

Veeravalli, S. & Warhaft, Z. 1989 The shearless turbulence mixing layer. *Journal of Fluid Mechanics*, 207, 191-229.

Voulgaris, G. & Trowbridge, J. H. 1998 Evaluation of the acoustic Doppler velocimeter (ADV) for turbulence measurements. *Journal of Atmospheric and Oceanic Technology*, 15, 272-289.

Westerweel, J., Fukushima, C., Pedersen, J. M. & Hunt, J. C. R. 2005 Mechanics of the turbulent/non-turbulent interface of a jet. *Physical Review Letters*, 95, 174501, 1-4.

Westerweel, J., Fukushima, C., Pedersen, J. M. & Hunt, J. C. R. 2009 Momentum and scalar transport at the turbulent/non-turbulent interface of a jet. *Journal of Fluid Mechanics*, 631, 199-230.

Wright, S. J. 1994 The effect of ambient turbulence on jet mixing. *In: Davies, P.A. and Valente Neves, M.I. (eds.), Recent Research Advances in the Fluid Mechanics of Turbulent Jets and Plumes, NATO ASI Series E*, 255, 13-27.

Wygnanski, I. & Fiedler, H. 1969 Some measurements in the self-preserving jet. *Journal of Fluid Mechanics*, 38, 577-612.

Xu, G. & Antonia, R. A. 2002 Effect of different initial conditions on a turbulent round free jet. *Experiments in Fluids*, 33, 677-683.

	Present work: stationary hot-film anemometry			Present work: flying hot-film anemometry			Present work: ADV			Wygnanski and Fiedler (1969): stationary hot-wire anemometry $x/D < 50$	Wygnanski and Fiedler (1969): stationary hot-wire anemometry $x/D > 50$	Panchapakesan and Lumley (1993): flying hot-wire anemometry	Hussein *et al.* (1994): stationary hot-wire anemometry	Hussein *et al.* (1994): laser-Doppler anemometry
Re	10,600			10,600			10,600			100,000		11,000	95,500	95,500
x_0/D	0	4	4.18	0	4	2.89	0	4	5.5	3	7	0	2.7	4
B	6.29	5.92	5.90	6.34	5.94	6.05	5.99	5.66	5.43	5.7	5	6.06	5.9	5.8
S	-			0.101			0.099			0.084		0.096	0.102	0.094

TABLE 1. The velocity decay constant (B), and spreading rate (S) for an axisymmetric turbulent jet. Because the value of the decay constant is sensitive to the virtual origin, B was calculated herein using the virtual origins of i) Panchapakesan and Lumley (1993) ($x_0/D = 0$), ii) Hussein, Capp and George (1994) ($x_0/D = 4$), and iii) the value obtained using a simultaneous least-square fit of both B and x_0 to the data. Note that radial profiles (and therefore the spreading rate) cannot be accurately measured using stationary hot-film anemometry because of the large turbulence intensities (and therefore flow reversals) at the edges of the jet. Adapted from Khorsandi *et al.* (2012).

Downstream distance [y/M]	u_α	$\langle U_\alpha \rangle$ [cm/s]	$u_{\alpha\,rms}$ [cm/s]	$\frac{\langle U_\alpha \rangle}{u_{\alpha\,rms}}$	Anisotropies $\frac{u_{rms}}{u_{\alpha\,rms}}$	$\frac{v_{rms}}{u_{\alpha\,rms}}$	$\frac{w_{rms}}{u_{\alpha\,rms}}$	S	K	$\frac{1}{2}\langle u_i u_i \rangle$	ℓ [cm]
5.5	u	0.61±0.05	2.31±0.03	0.27±0.02	1	1.23	–	0.39±0.09	5.42±0.62	9.33±0.06	6.8
	v	0.31±0.13	2.84±0.04	0.11±0.04	0.81	1	–	1.18±0.06	4.6±0.40		
	w	–	–	–	–	–	–	–	–		
7.3	u	0.03±0.18	1.53±0.02	0.07±0.08	1	1.36	0.97	0.07±0.16	4.51±0.01	4.44±0.15	11.1
	v	-0.30±0.17	2.08±0.14	-0.15±0.10	0.73	1	0.72	1.43±0.12	5.73±0.66		
	w	0.10±0.10	1.49±0.05	0.07±0.07	1.03	1.40	1	-0.18±0.08	4.05±0.21		

TABLE 2. Background turbulence conditions at $y/M = 5.5$ and $y/M = 7.3$ ($M = 150$ mm). Note that u is measured with the flying hot-film and v and w are measured with the z-component of the ADV. The statistics for w at $y/M = 5.5$ were not measured, so the turbulent kinetic energy ($\frac{1}{2}\langle u_i u_i \rangle$) was calculated as $\frac{1}{2}(\langle u^2 \rangle + \langle v^2 \rangle + \langle u^2 \rangle$, due to the symmetry of the RJA flow at that downstream location. The integral length scale, $\ell \equiv \int_0^\infty \rho_{uu}(x)$, is calculated from the spatial autocorrelation of u, $\rho_{uu}(x)$, measured in the background turbulence along a line parallel to the RJA.

	Jet in quiescent background	Jet+RJA (TKE = 4.44 cm^2/s^2)	Jet+RJA (TKE = 9.33 cm^2/s^2)
Re = 10,600	$x^{-1.06}$	$x^{-1.83}$, for $x/D \leq$ 50	$x^{-2.13}$, for $x/D \leq$ 50
Re = 5,800	$x^{-1.17}$, for $x/D \leq$ 60	$x^{-2.50}$, for $x/D \leq$ 45	$x^{-3.38}$, for $x/D \leq$ 40
Re = 5,300	$x^{-1.06}$, for $x/D \leq$ 60	$x^{-2.57}$, for $x/D \leq$ 30	$x^{-4.34}$, for $x/D \leq$ 25

TABLE 3. Decay constants for jet in both quiescent and turbulent backgrounds.

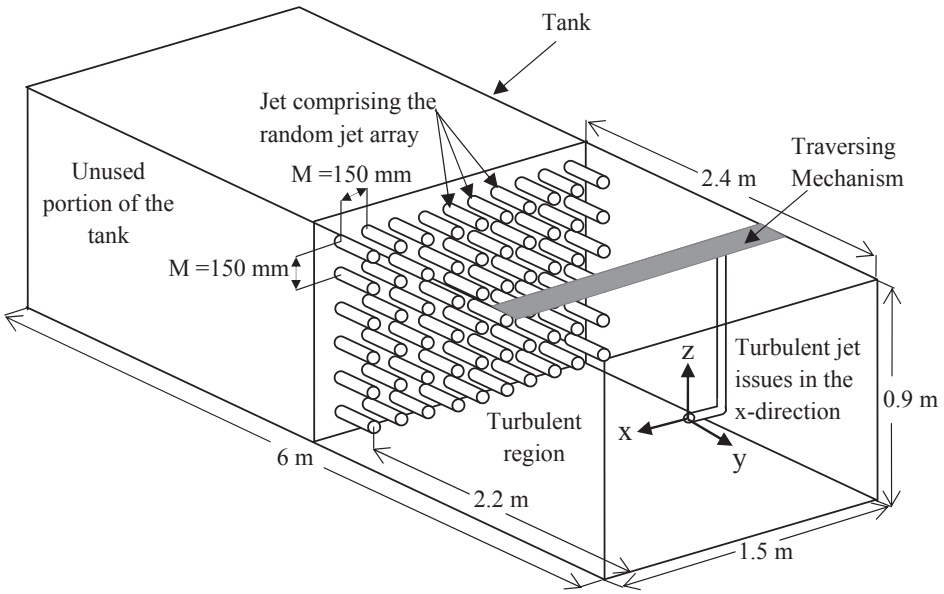

FIGURE 1. Schematic of the jet, RJA, and tank. (Not to scale.)

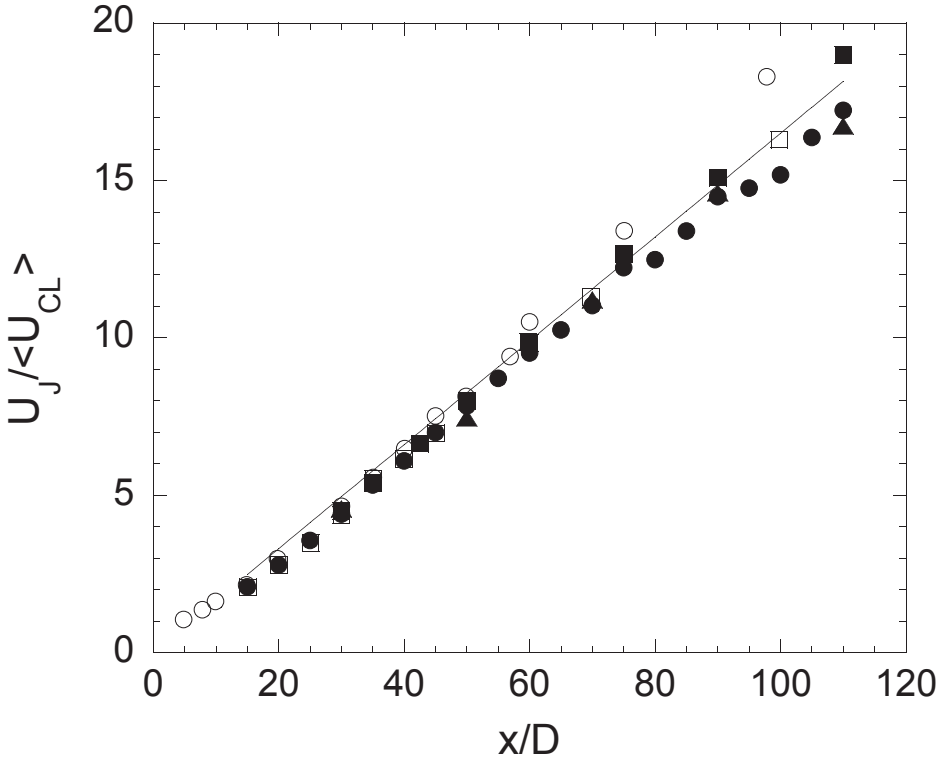

FIGURE 2. Downstream evolution of the centreline axial mean velocity of an axisymmetric turbulent jet at Re = 10,600 emitted into a quiescent background. Note that no virtual origin is used for the data sets in this figure (as their values are inferred from this plot). Solid symbols represent the present work: ▲, SHFA; ●, FHFA; ■, ADV. ○, SHWA data of Wygnanski and Fiedler (1969); solid line, FHWA data of Panchapakesan and Lumley (1993); □, SHWA data of Hussein, Capp and George (1994). Adapted from Khorsandi *et al.* (2012).

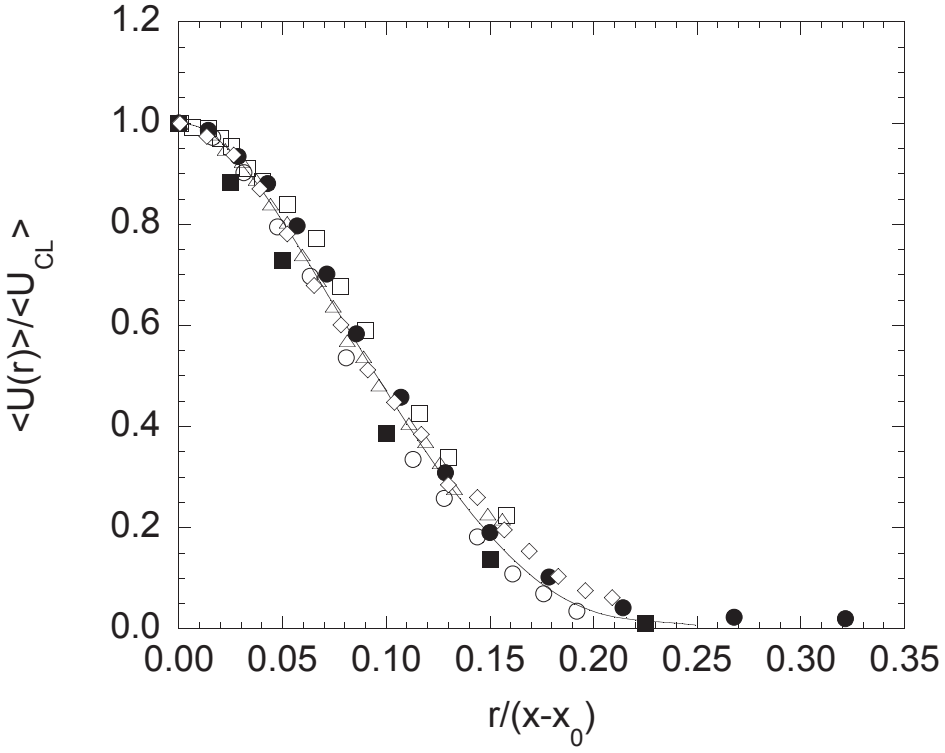

FIGURE 3. Radial profile of the mean axial velocity of an axisymmetric turbulent jet at $Re =$ 10,600 ($x/D = 35$; $x_0/D = 0$). Solid symbols represent the present work: •, FHFA; ■, ADV. ○, SHWA data of Wygnanski and Fiedler (1969) having $x_0/D = 0$; solid line, FHWA data of Panchapakesan and Lumley (1993) having $x_0/D = 0$; □, SHWA data of Hussein, Capp and George (1994) having $x_0/D = 4$; △, FHWA data of Hussein, Capp and George (1994) having $x_0/D = 4$; ◇, LDA data of Hussein, Capp and George (1994) having $x_0/D = 4$. Adapted from Khorsandi *et al.* (2012).

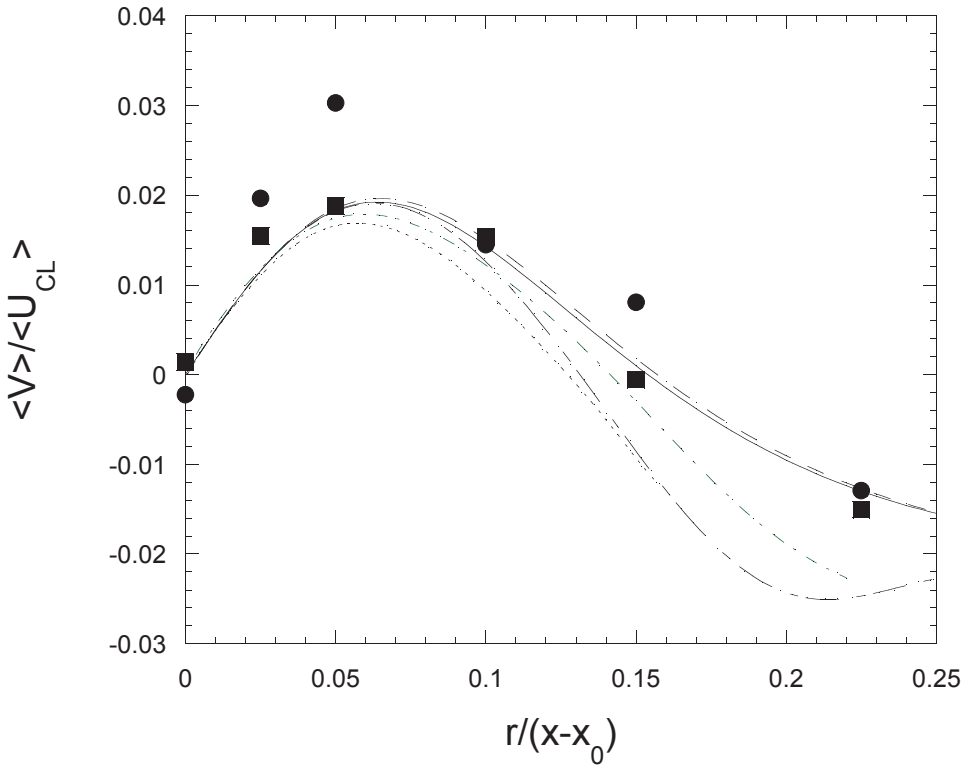

FIGURE 4. The mean radial velocity profile of an axisymmetric turbulent jet at Re = 10,600. Solid symbols represent the present raw data: •, ADV $x/D = 35$ with $x_0/D = 0$; ■, ADV $x/D = 75$ with $x_0/D = 0$. Note that the lines are the profiles obtained from the axial mean velocity profile using the continuity equation: —, Present work ADV; - -, Present work FHFA. · · ·, SHWA data of Wygnanski and Fiedler (1969); - —, FHWA data of Panchapakesan and Lumley (1993); · –, LDA data of Hussein, Capp and George (1994).

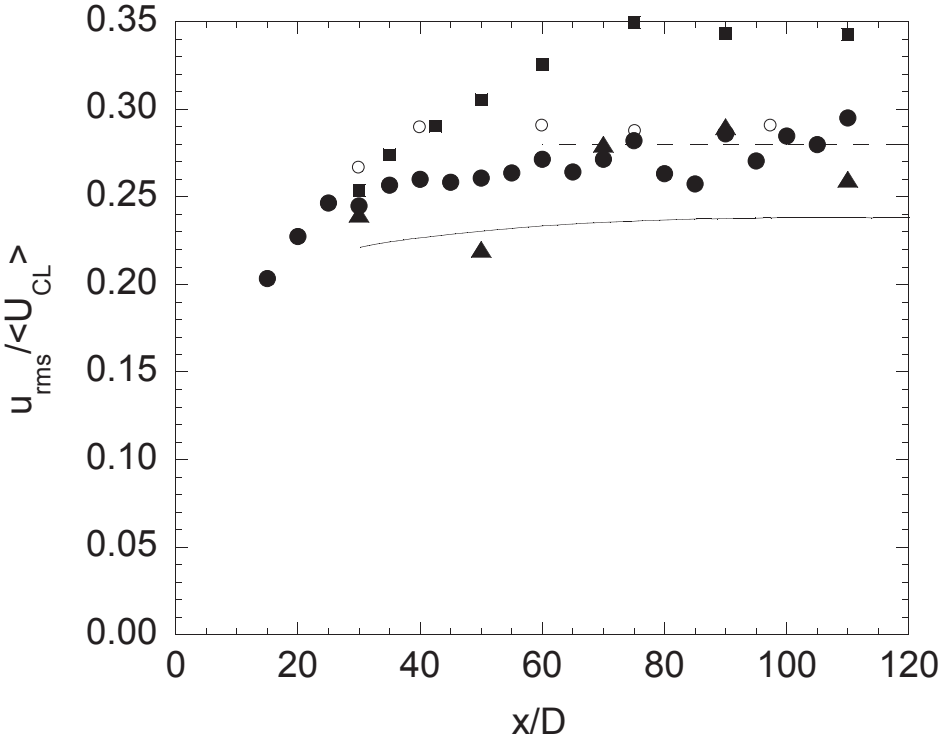

FIGURE 5. Downstream evolution of the axial RMS velocity at the centreline of the jet at Re = 10,600. Solid symbols represent the present work: ▲, SHFA; ●, FHFA; ■, ADV. ○, SHWA data of Wygnanski and Fiedler (1969); solid line, FHWA data of Panchapakesan and Lumley (1993); broken line, SHWA and LDA data of Hussein, Capp and George (1994). Adapted from Khorsandi *et al.* (2012).

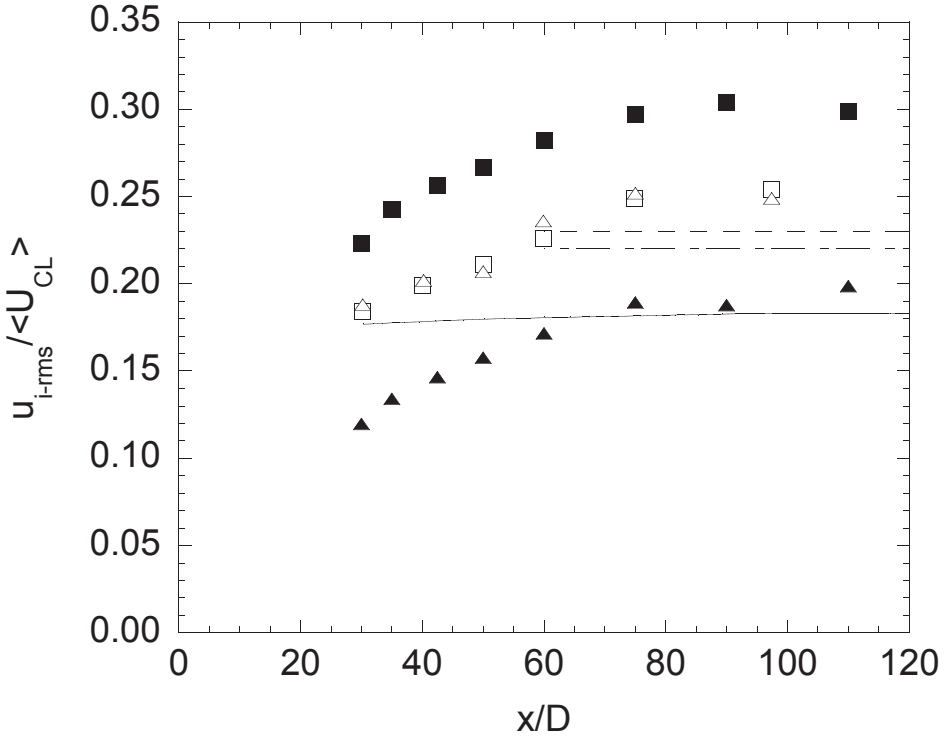

FIGURE 6. Downstream evolution of the lateral RMS velocities at the centreline of the jet at Re = 10,600. Solid symbols represent the present work: v_{rms}: ■, w_{rms}: ▲, ADV. v_{rms}: □, w_{rms}: △, SHWA data of Wygnanski and Fiedler (1969); solid line, FHWA data of Panchapakesan and Lumley (1993); - —, SHWA data of Hussein, Capp and George (1994); - -, LDA data of Hussein, Capp and George (1994). Adapted from Khorsandi *et al.* (2012).

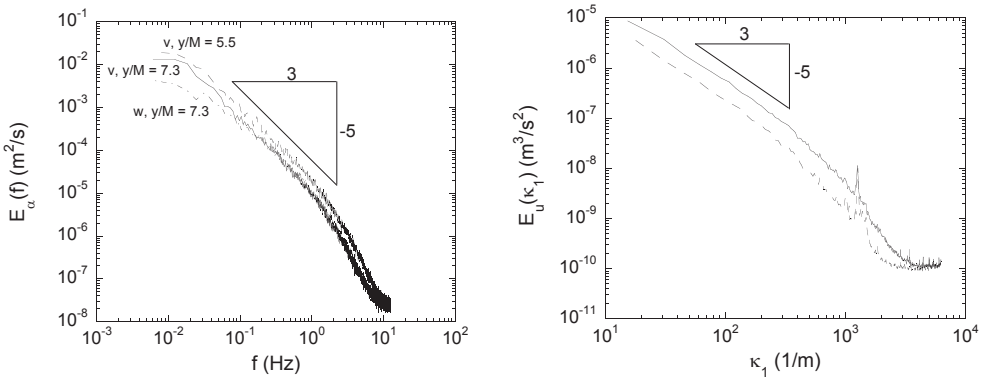

FIGURE 7. (a) Eulerian temporal velocity spectra measured by ADV in the turbulent background. $E_v(f)$ at $y/M = 5.5$: dashed line. $E_v(f)$ at $y/M = 7.3$: solid line. $E_w(f)$ at $y/M = 7.3$: dot-dashed line. (b) Eulerian spatial velocity spectra measured by flying hot-film anemometry in the turbulent background. κ_1 is the longitudinal wavenumber. $E_u(\kappa_1)$ at $y/M = 5.5$: solid line. $E_u(\kappa_1)$ at $y/M = 7.3$: dashed line.

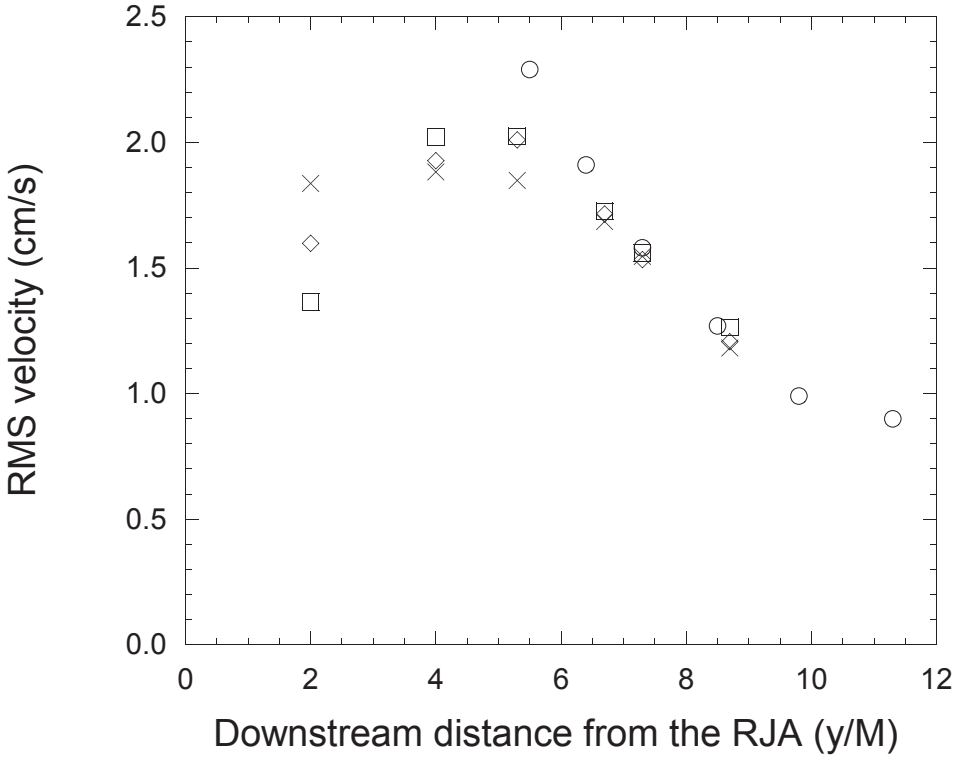

FIGURE 8. Decay of the RMS velocities in the background turbulence as a function of downstream distance from the RJA. ○, u_{rms} measured by FHFA moving between two rows of jets, -3 $< x/M <$ 2, $z/M = 0$; □, w_{rms} measured by ADV centred between four jets, (x/M, Z/M) = (0, 0); ◇, w_{rms} measured by ADV centred between two jets, (x/M, Z/M) = (0, 0.5); ×, w_{rms} measured by ADV in front of a jet, (x/M, Z/M) = (-0.5, 0.5).

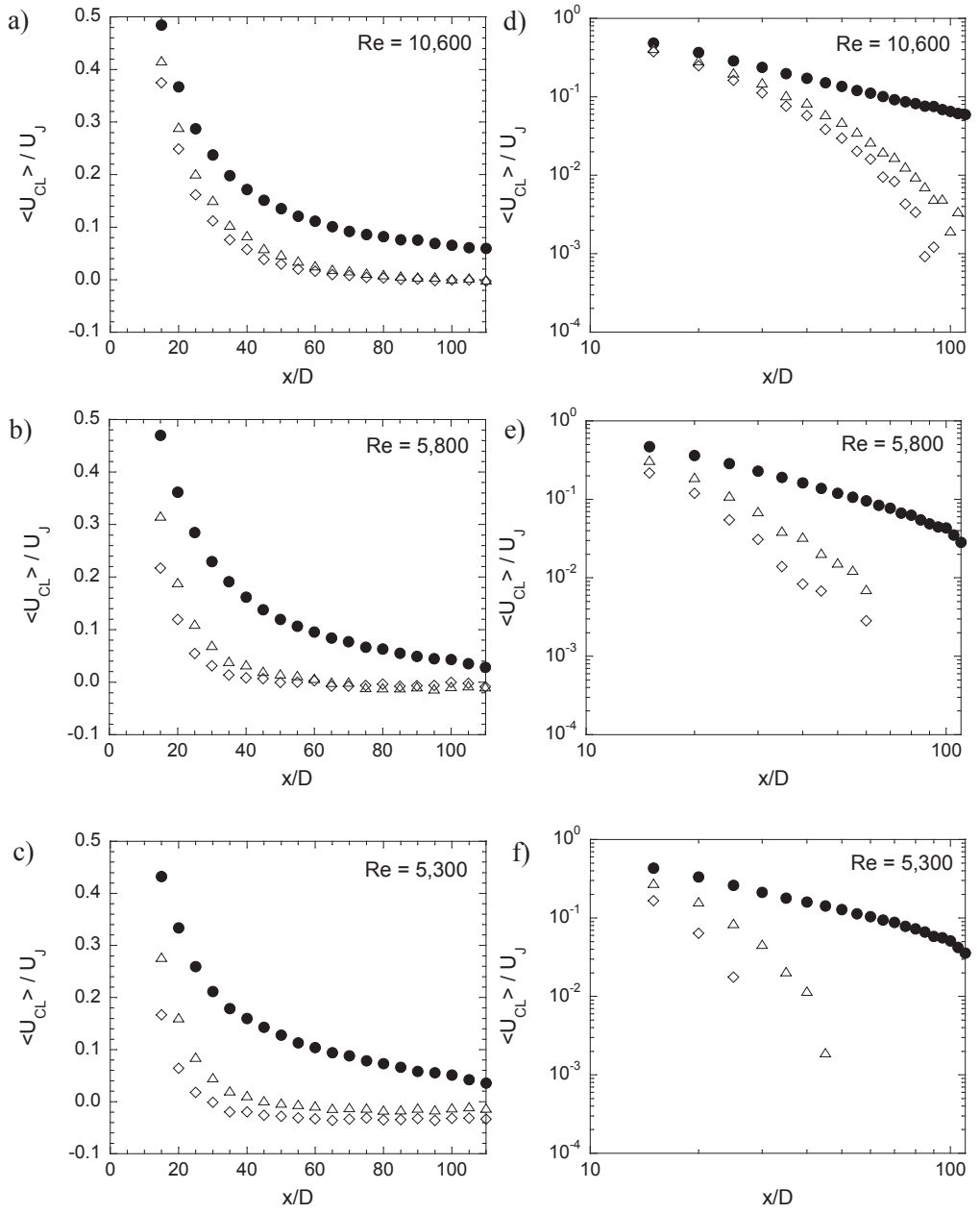

FIGURE 9. The effect of background turbulence on the downstream evolution of the mean axial velocity of an axisymmetric turbulent jet: a) Re = 10,600, b) Re = 5,800, and c) Re = 5,300, Linear-linear coordinates; d) Re = 10,600, e) Re = 5,800, and f) Re = 5,300, Log-log coordinates. •, Jet; △, Jet+RJA, TKE = 4.44 cm^2/s^2; ◇, Jet+RJA, TKE = 9.33 cm^2/s^2.

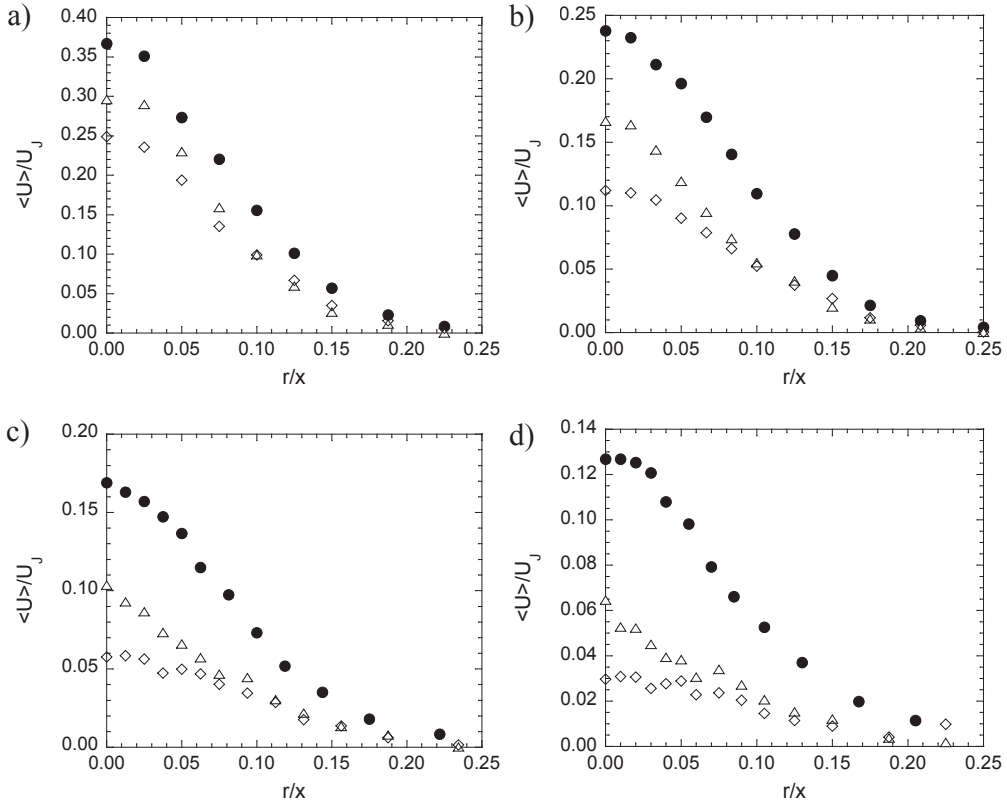

FIGURE 10. The effect of background turbulence on the radial profile of mean axial velocity of an axisymmetric turbulent jet at Re = 10,600: a) $x/D = 20$, b) $x/D = 30$, c) $x/D = 40$, and d) $x/D = 50$. •, Jet; △, Jet+RJA, TKE = 4.44 cm^2/s^2; ◇, Jet+RJA, TKE = 9.33 cm^2/s^2.

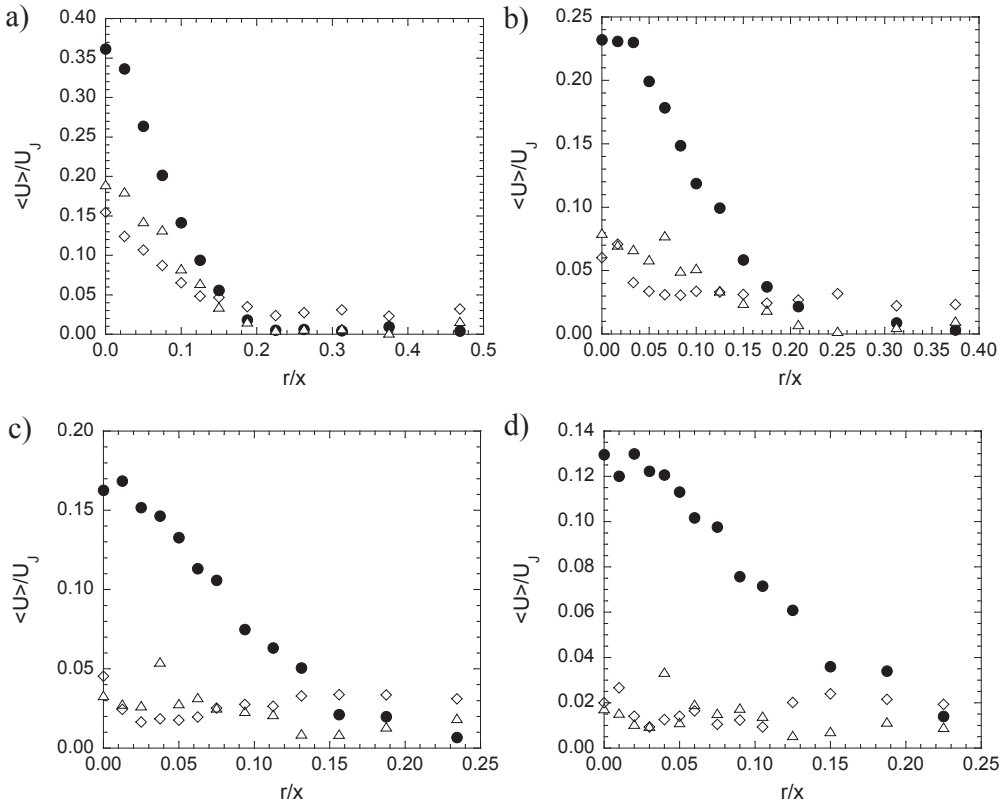

FIGURE 11. The effect of background turbulence on the radial profile of mean axial velocity of an axisymmetric turbulent jet at $Re = 5{,}800$: a) $x/D = 20$, b) $x/D = 30$, c) $x/D = 40$, and d) $x/D = 50$. •, Jet; △, Jet+RJA, TKE = 4.44 cm^2/s^2; ⋄, Jet+RJA, TKE = 9.33 cm^2/s^2.

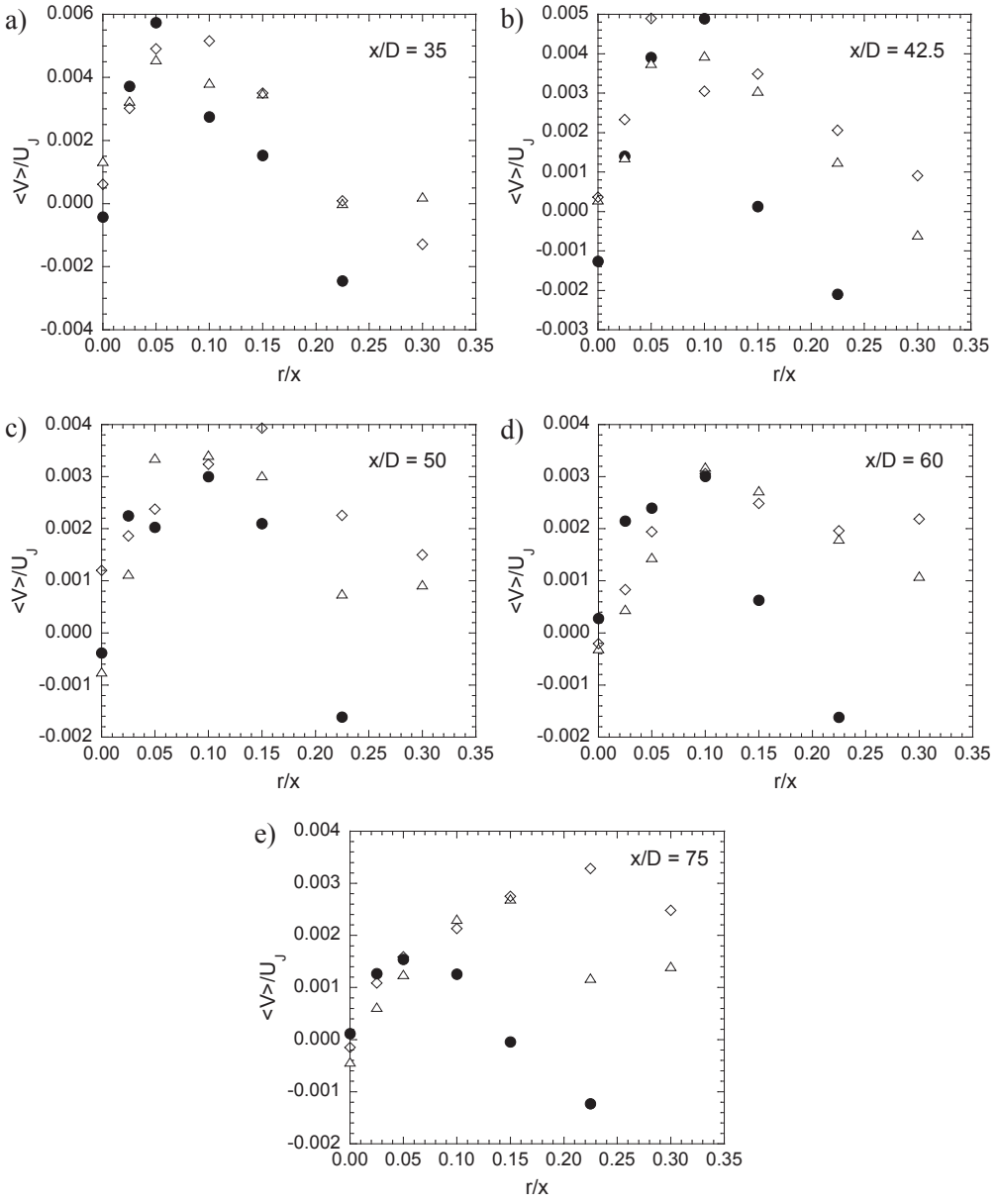

FIGURE 12. The effect of background turbulence on the radial profile of the mean radial velocity of an axisymmetric turbulent jet at Re = 10,600: a) $x/D = 35$, b) $x/D = 42.5$, c) $x/D = 50$, d) $x/D = 60$, and e) $x/D = 75$. •, Jet; △, Jet+RJA, TKE = 4.44 cm^2/s^2; ◇, Jet+RJA, TKE = 9.33 cm^2/s^2.

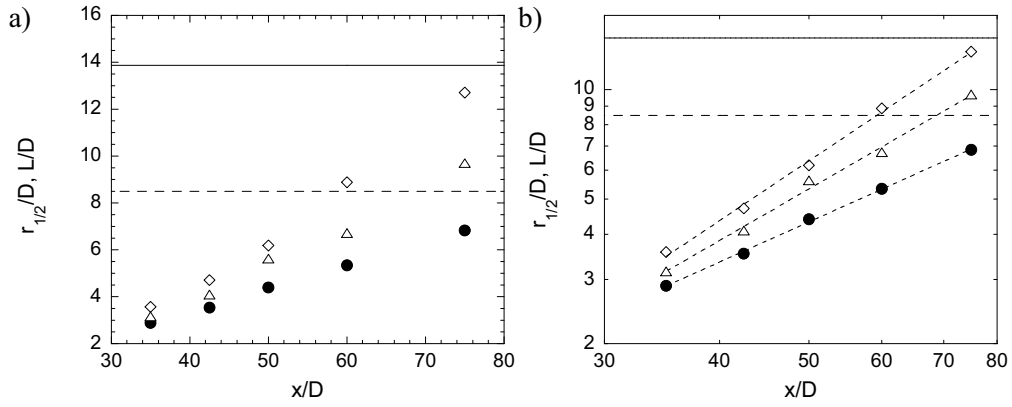

FIGURE 13. The effect of background turbulence on the downstream evolution of the half-width of an axisymmetric turbulent jet (Re = 10,600). a) Linear-linear coordinates. b) Log-log coordinates. •, Jet; △, Jet+RJA, TKE = 4.44 cm^2/s^2; ◇, Jet+RJA, TKE = 9.33 cm^2/s^2; —, ℓ/D RJA, TKE = 4.44 cm^2/s^2; - -, ℓ/D RJA, TKE = 9.33 cm^2/s^2.

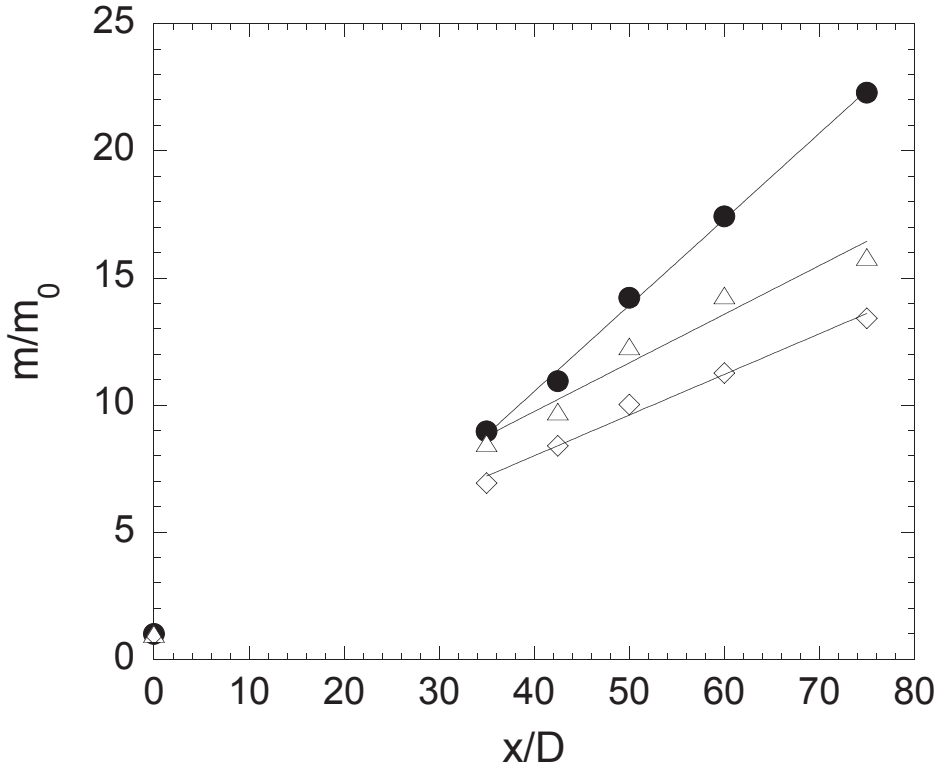

FIGURE 14. The effect of background turbulence on the downstream evolution of the mass flow rate of an axisymmetric turbulent jet. •, Jet; △, Jet+RJA, TKE = 4.44 cm^2/s^2; ◇, Jet+RJA, TKE = 9.33 cm^2/s^2.

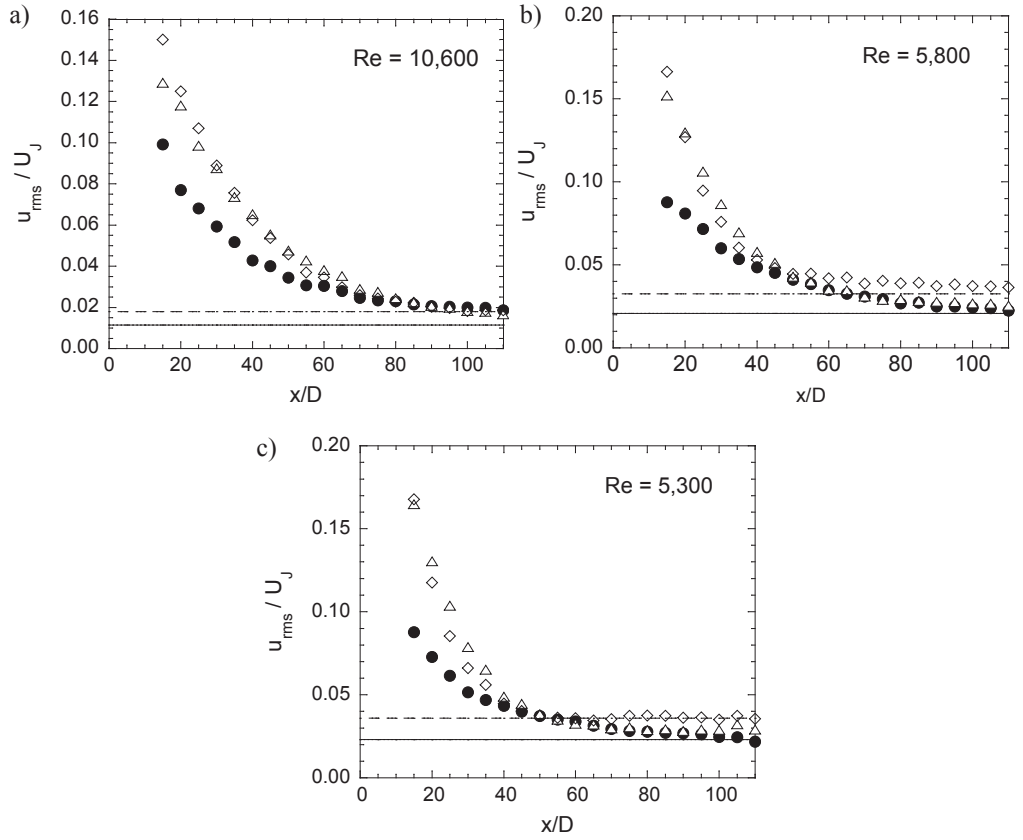

FIGURE 15. Downstream evolution of the RMS axial velocities at the centreline of the jet (normalized by the exit velocity of the jet, U_J) in quiescent and turbulent backgrounds: a) Re = 10,600, b) Re = 5,800, and c) Re = 5,300. •, Jet; △, Jet+RJA, TKE = 4.44 cm^2/s^2; ⋄, Jet+RJA, TKE = 9.33 cm^2/s^2; —, RJA, TKE = 4.44 cm^2/s^2; - -, RJA, TKE = 9.33 cm^2/s^2.

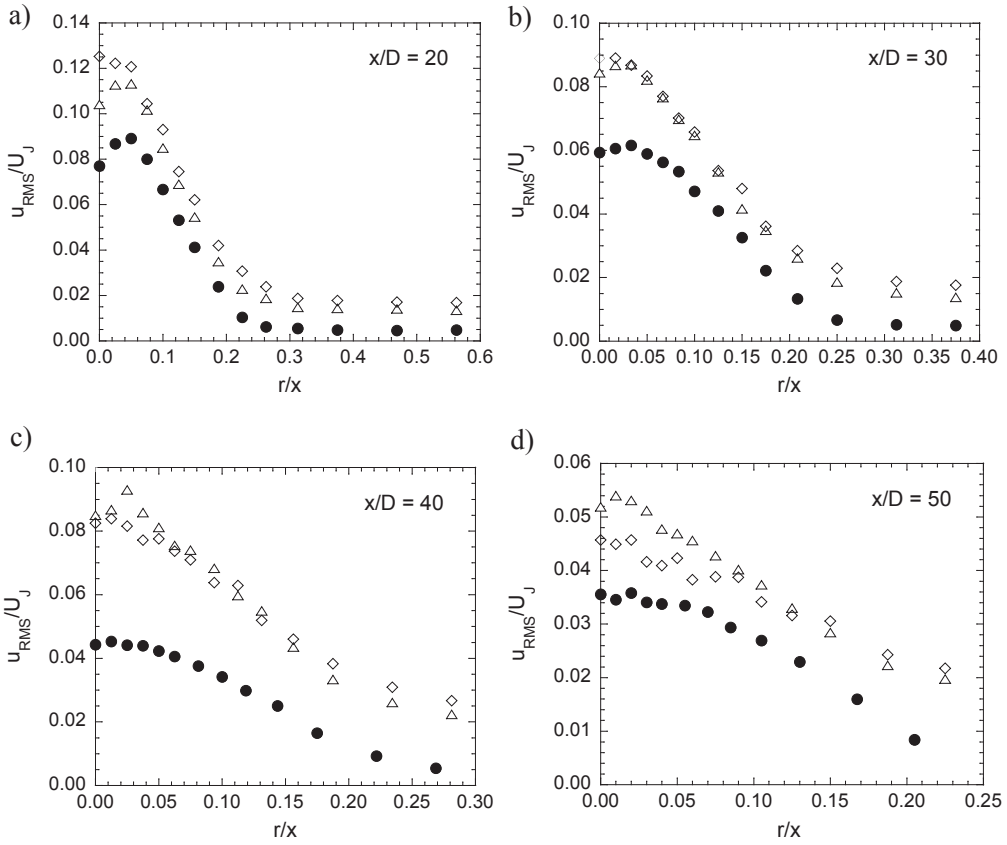

FIGURE 16. The effect of background turbulence on the radial profiles of the RMS axial velocity of an axisymmetric turbulent jet at Re = 10,600: a) $x/D = 20$, b) $x/D = 30$, c) $x/D = 40$, and d) $x/D = 50$. •, Jet; △, Jet+RJA, TKE = 4.44 cm^2/s^2; ⋄, Jet+RJA, TKE = 9.33 cm^2/s^2.

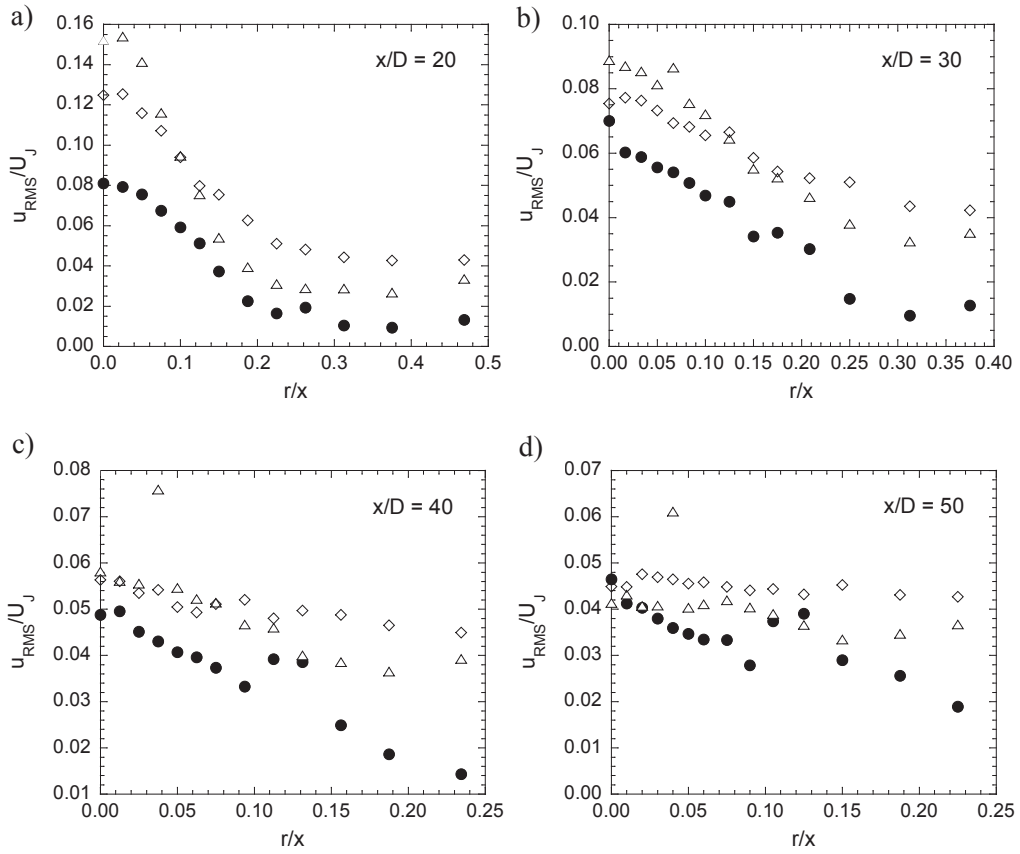

FIGURE 17. The effect of background turbulence on the radial profiles of the RMS axial velocity of an axisymmetric turbulent jet at $Re = 5{,}800$: a) $x/D = 20$, b) $x/D = 30$, c) $x/D = 40$, and d) $x/D = 50$. •, Jet; △, Jet+RJA, TKE = 4.44 $\mathrm{cm}^2/\mathrm{s}^2$; ◇, Jet+RJA, TKE = 9.33 $\mathrm{cm}^2/\mathrm{s}^2$.

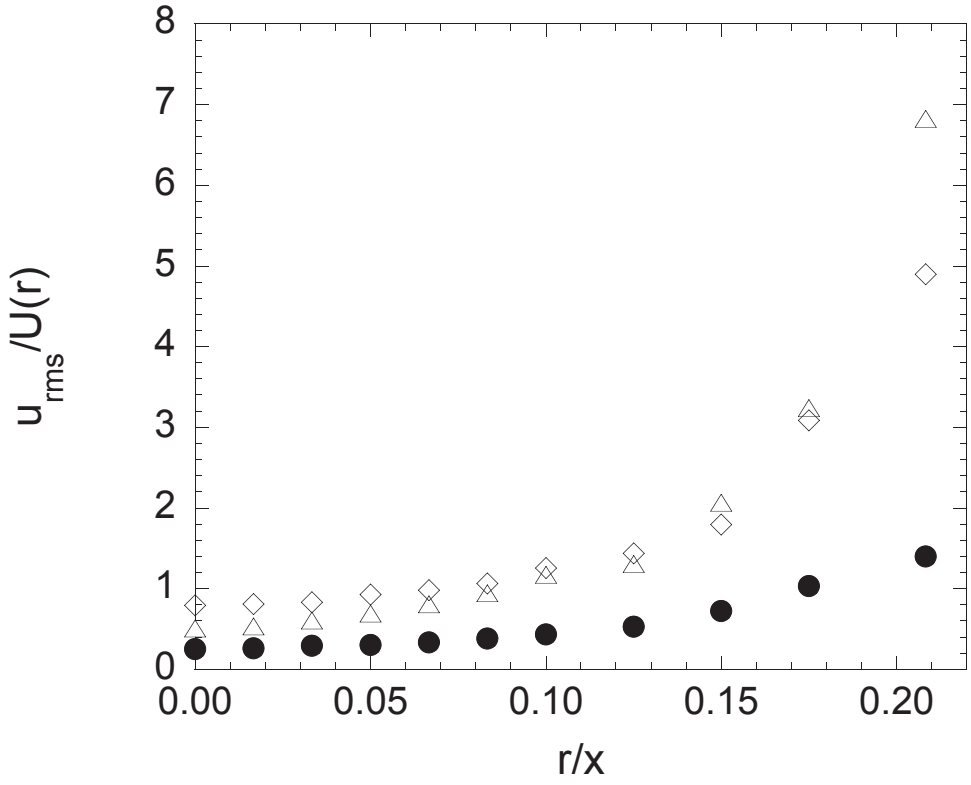

FIGURE 18. The effect of background turbulence on the profile of the radial local turbulence intensity $x/D = 30$, $Re = 10{,}600$. •, Jet; △, Jet+RJA, TKE = 4.44 $\mathrm{cm}^2/\mathrm{s}^2$; ◇, Jet+RJA, TKE = 9.33 $\mathrm{cm}^2/\mathrm{s}^2$.

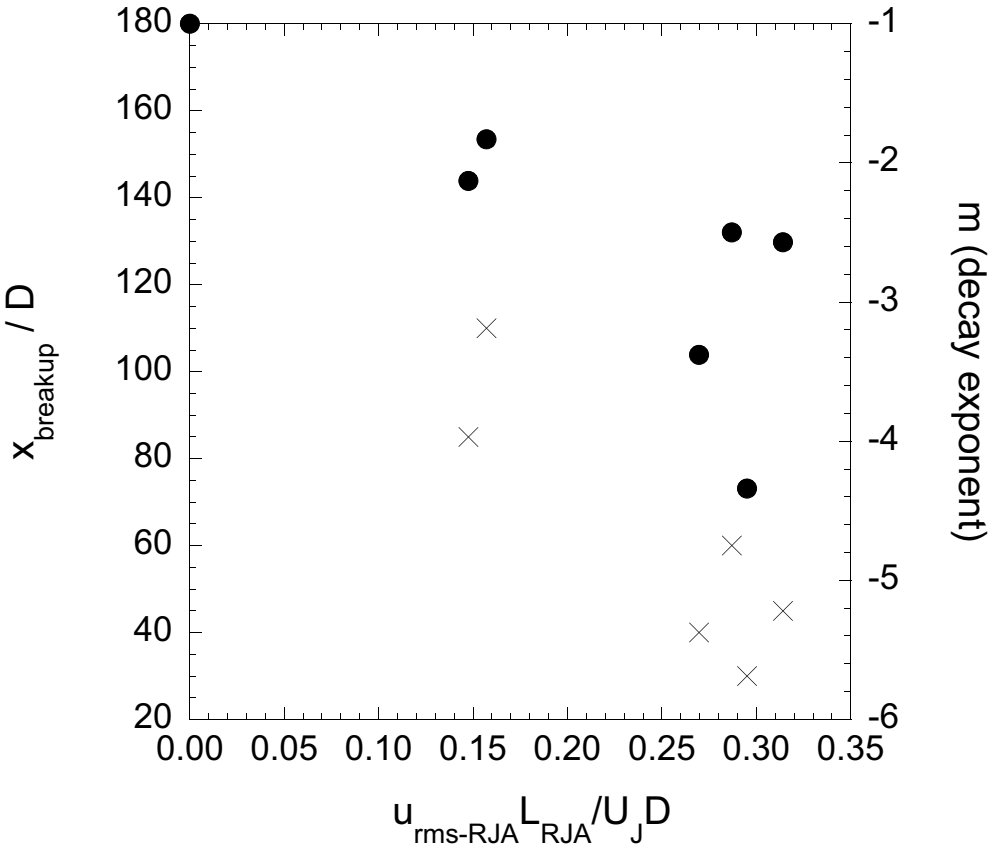

FIGURE 19. Breakup location of the jet determined from the mean velocity field (×) and decay exponents of the centreline mean velocity (•) as a function of the ratio of the Reynolds numbers of the background turbulence and the jet.

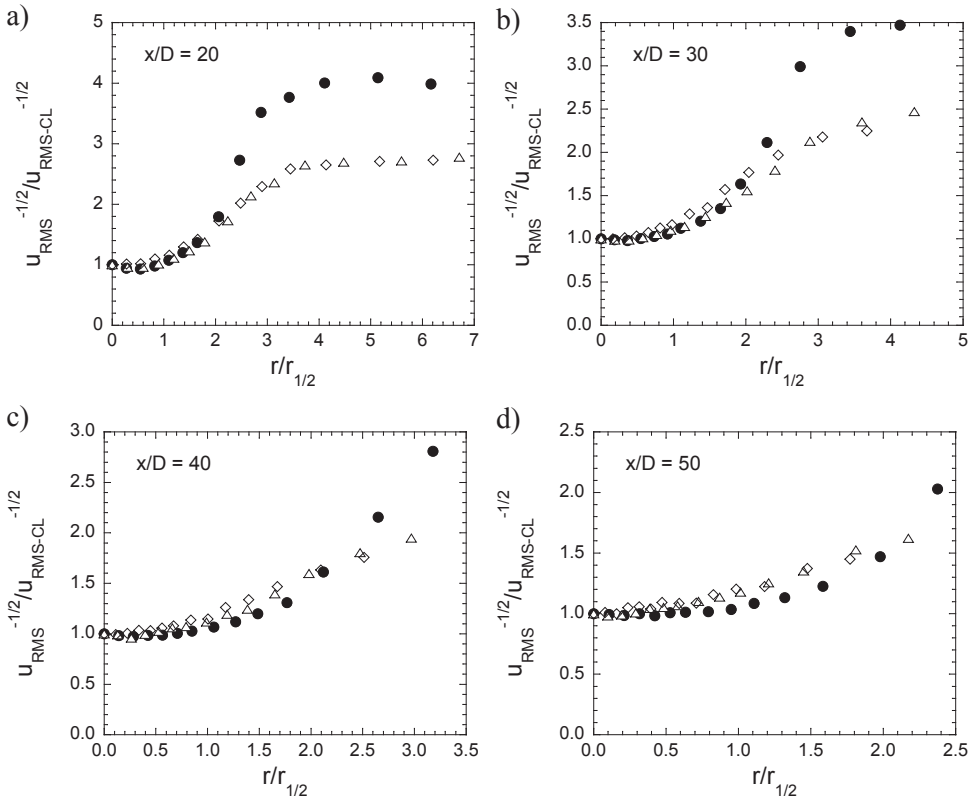

FIGURE 20. Test of Phillips's first relation. $Re = 10,600$. •, Jet; △, Jet+RJA, TKE = 4.44 $\mathrm{cm}^2/\mathrm{s}^2$; ◇, Jet+RJA, TKE = 9.33 $\mathrm{cm}^2/\mathrm{s}^2$. (a) $x/D = 20$.(*b*)x/D=30. (c) $x/D = 40$.(*d*)x/D=50.